AD-786 951

DEFENSE NUCLEAR AGENCY REACTION RATE HANDBOOK. SECOND EDITION. REVISION NUMBER 2

General Electric Company
Philadelphia, Pennsylvania

May 1974

MEMORANDUM

To: All Authorized Recipients of the DNA Reaction Rate Handbook (DNA 1948H)

From: The Editors

Subject: Revision Number 2

Enclosed herewith you will find a copy of Revision Number 2 to the Handbook. It comprises the newly written Chapter 22. Related revisions to appropriate pages of the introductory matter and the Appendices will be included in a later revision.

You should immediately substitute the enclosed items into your copy of the Handbook, discarding old pages 22-1 and 22-2.

You should also enter on page iii in front of your Handbook the following information: Revision No. 2; Date of Issue—May 1974; Date of Receipt—whatever day you receive this; and sign your name in the last column.

Revision Number 3 has already been issued. Revision Number 4 is expected to be issued during the late summer or early fall of 1974. Thank you for your cooperation.

It will be noted that, as these revisions continue to be issued, some of the Handbook appendices will tend to become outdated. From time to time revisions to the appendices will be distributed, in order to correct this situation.

22. APPLICATIONS OF COMPUTER SOLUTIONS TO ATMOSPHERIC DEIONIZATION PROCESSES

A.W. Ali, Naval Research Laboratory
W.S. Knapp, General Electric—TEMPO
F.E. Niles, Ballistic Research Laboratories

(Latest Revision 5 March 1974)

22.1 INTRODUCTION

Many natural and man-made events entail disturbances of the upper atmosphere. Of particular interest is the sequence of deionization phenomena following a nuclear burst. The radiation and debris from a nuclear burst interact with the ambient atmosphere in the three environmental regions listed in Chapter 1, viz., (1) the fireball region, (2) the fireball halo or the UV fireball, and (3) the cool disturbed region beyond. This interaction results in a disturbed atmosphere with varying degrees of ionization and additional species which are not present or are very minor under normal conditions. These disturbed regions can be described mathematically with an appropriate computer code designed for a specific function. In general one is interested in the time histories of the species in the disturbed regions and the time histories of the electron temperature, the vibrational temperature, and the heavy-particle (neutral) temperature. Thus rate equations are written for each species and the desired temperatures. Then these equations are solved using some type of numerical integration technique to obtain the desired quantities as a function of time. Codes with many species are known as multi-species codes.

However, to describe the deionization of a disturbed region by an appropriate code one must know the source of the disturbance, its duration, the atmospheric species densities, and basic physical and chemical processes involved. (See Chapter 6 for a discussion of the chemical kinetics of the disturbed atmosphere.)

On the other hand the complexity of a code, e.g., the number of species, temperatures, reactions, and other desired quantities depends on:

(a) The purpose for which the code is designed, i.e., whether the code is to be used for radar propagation, communication, or optical systems studies, or for some or all of these purposes simultaneously.

(b) Whether the code is to be used in conjunction with hydrodynamic codes.

(c) Computational time requirements and the size of the computer, since the time required to perform detailed deionization calculations could be prohibitive where solutions are needed at thousands of points in space and time.

No computer code can include all of the possible reactions which may occur, especially when each energetic state of a constituent should be considered as a separate species with its own reactions. One hopes, however, that the principal species and reactions are identified and included. In this chapter several multispecies codes for the D, E, and F regions are discussed. The dominant reactions and the important species are pointed out for each region.

Numerical methods for solving the rate equations are reviewed. Simplified codes with physical and mathematical approximations and the lumped-parameter method are also discussed.

22.2 NUMERICAL METHODS FOR SOLVING THE RATE EQUATIONS

The rate equations for n species are a set of n first-order, coupled, and generally nonlinear differential equations. Given a set of chemical reactions involving the n species and specifications for the concentrations, $n_{0,i}$, at time t_0 for the i'th species, the requirement becomes one of generating a set of n differential equations and solving the set numerically for time greater than t_0.

The differential equations may be written as:

$$\frac{dn_i}{dt} = f_i - \frac{n_i}{t_i} \quad , \tag{22-1}$$

where f_i is the rate of formation of the i'th species and $(t_i)^{-1}$ is the removal frequency of the same species.

If f_i and t_i are constants, Equation (22-1) can be solved analytically to yield:

$$n_i(t) = f_i t_i + (n_{0,i} - f_i t_i) \exp\left[-(t - t_0)/t_i\right] \quad . \tag{22-2}$$

Equation (22-2) reveals that $1/t_i$ describes how quickly the concentration of the i'th species reaches its equilibrium value of $f_i t_i$ with a characteristic time of t_i.

Unfortunately f_i and t_i are normally functions of time and the differential equations most often encountered have time constants for the different species which vary over many orders of magnitude. Often the shorter time constants are much shorter than the time step desired for performing the numerical integration. For the classical methods of numerical integration, the solutions become unstable if for the largest $(t_i)^{-1}$, denoted as R, the product of R and the time step of integration, h, is greater than some small quantity which is typically near one, i.e., $Rh \gtrsim 1$. The equations for which $(t_i)^{-1}h$ is $\gtrsim 1$ are said to be numerically stiff. When this is the case, the problem of integration becomes more complex and nonclassical methods (which are free of the constraints that $(t_i)^{-1}h \lesssim 1$) must be adopted in order to obtain solutions within a reasonable amount of computer time. The nonclassical methods must confront two major restraints, viz., accuracy and stability.

The nonclassical methods fall into two classes: those which treat all the differential equations in the same manner and those which recognize the stiff equations and integrate them by a stable method with the rest of the equations being integrated by a more accurate, but less stable, classical method. We shall refer to the latter class as "hybrid methods."

In all hybrid methods two important considerations must be addressed. The first is the establishment of a criterion to determine by which method specific equations are to be integrated. The second is how the chemical balance and charge balance are to be maintained and how much imbalance will be allowed. Hybrid methods are reasonably fast; however, the accumulated errors may become large after many time steps so that care must be exercised in using them. Kuneshea (Reference 22-1) has developed and utilized a hybrid method in his codes.

The main ideas behind the classical methods along with a survey and discussion of the literature have been given by Benyon (Reference 22-2). He has given comparisons for predictor, predictor-corrector, and Runge-Kutta methods and has listed 75 references. Also he has provided a few comments regarding nonclassical methods. Several books have been written on methods of solving differential equations.

A few of these are listed among the references at the end of this chapter (References 22-3 through 22-21).

Among the nonclassical methods of principal interest for atmospheric deionization calculations are: the hybrid method of Keneshea (Reference 22-1), the algorithm of Treanor (Reference 22-22), the explicit method of Fowler and Warten (Reference 22-23), the selected order, multistep predictor-corrector method of Gear (Reference 22-24), the matrix method of Kregel (Reference 22-25), and the CHEMEQ Stiff Equation Integrator by Young and Boris (Reference 22-26).

Young and Boris (Reference 22-26) have devised their method for the purpose of extremely fast numerical solution in the chemistry rate equations of the deionization type while maintaining a moderate level of accuracy, and for coupling rate equations to the general flows arising in disturbed atmospheric phenomena.

In selecting the method to be used, one obviously wants that which will require the least amount of computer time while maintaining an acceptable accuracy. A direct comparison of methods is complicated by the fact that they may not all be optimized in the coding for the computer being used for the comparison study. A poor method for a given application may run faster than a better method when the poor method is coded using optimum coding practices. Examples of non-optimum coding practices include: (1) using doubly subscripted variables when a singly subscripted variable could be used; and (2) passing information in and out of subroutines of functions using the linkage rather than the use of COMMON when COMMON could be used.

In addition to considering which method of numerical integration is best and the use of optimized coding practices, one must consider: (1) how to compute or estimate the error per time step; (2) criteria for changing step size; (3) how much the step size should be changed when it is changed; (4) how to conserve chemical balance; (5) how to conserve charge balance; and other factors. In many cases these considerations can be addressed only by trial and error.

All methods which do not conserve chemical balance and charge balance automatically may be made to do so by at least two techniques. First, balance can be invoked by summing the various concentrations to find the errors and then distributing the errors throughout the densities in such a way that balance is conserved. The major fault

with this technique is that one is incorporating a portion of the errors into concentrations from which the errors may not have arisen. A second, better method, but one which is not always practical, is to take the concentrations generated at each step and use these as input into a final step which does conserve balance automatically.

The success of multispecies codes for atmospheric deionization depends, in addition to an appropriate description of the physics and chemistry of the ionized atmosphere, on having fast, accurate methods of numerical integration.

22.3 MULTISPECIES CODES

22.3.1 The Disturbed E and F Regions Multispecies Codes

To describe the deionization in these disturbed regions, it is instructive to know that the dominant ambient constituents of the E and F regions are O, N_2, and O_2. The disturbing source, whether it is radiation or energetic particles, will create electrons and O^+, N_2^+, O_2^+, and N^+ as the dominant ions. The last ion arises either from dissociative ionization of N_2 or by the ionization of the products of the dissociative recombination of N_2^+. This last ionization process is generally the dominant source of N^+ during the presence of the disturbing radiation. Minor species, notably NO, are also ionized. Therefore, in principle one may write rate equations for all the above species, include physical and chemical processes, use the appropriate rate coefficients (see Chapter 24), assume a temperature, and thus have a deionization code. The question to ask at the outset, however, is whether this code would give the <u>right</u> electron density. To answer this question, let us examine the basic deionization processes which occur. The following dissociative recombinations:

$$N_2^+ + e \rightarrow N + N \qquad (22\text{-}3)$$

$$O_2^+ + e \rightarrow O + O \qquad (22\text{-}4)$$

$$NO^+ + e \rightarrow N + O \qquad (22\text{-}5)$$

are the most important processes which remove electrons. The first two reactions occur at early stages of the deionization while reaction (22-5) becomes important at late times. These reactions depend on

the electron temperature (Reference 22-27) as well as the ion-kinetic temperature (Reference 22-28)(actually the vibrational temperature). The next important reactions are the processes which remove an atomic ion and replace it by a molecular ion, i.e., ion-molecule rearrangement or charge-exchange collisions such as:

$$O^+ + N_2 \rightarrow NO^+ + N \qquad (22\text{-}6)$$

$$N^+ + O_2 \rightarrow NO^+ + O$$

$$\rightarrow O_2^+ + N \qquad (22\text{-}7)$$

$$O^+ + O_2 \rightarrow O_2^+ + O \qquad (22\text{-}8)$$

$$N^+ + NO \rightarrow NO^+ + N \qquad (22\text{-}9)$$

Reaction (22-6) is widely studied and it depends both on the nitrogen-vibrational temperature (Reference 22-29) and the ion-kinetic temperature (Reference 22-30). In a completely dissociated and ionized region, on the other hand, where only atomic ions are present, collisional radiative recombination is the only available deionization route. The processes discussed above indicate the importance of the electron, the nitrogen-vibrational, and the heavy-particle temperatures. Reaction (22-9), for example, depends on the formation of NO, which in turn depends on the heavy-particle temperature through the reaction of ground-state atomic nitrogen and molecular oxygen (see Chapter 24). However, the formation of NO proceeds faster if the reactant atomic nitrogen was in the (^{2}D) excited state (see Chapter 24). This illustrates the importance of metastable states in the deionization process.

In addition to the importance of N(^{2}D) in the formation of NO, it is also a source of electron heating by superelastic collisions. The same can be said for O(^{1}D) which is additionally quenched by N_2 (Reference 22-31) with almost all its internal energy being converted (Reference 22-32) into kinetic energy and not into vibrational energy of N_2 as was speculated earlier (Reference 22-33). However, a small amount of the O(^{1}D) energy may still end up in the vibrational mode of N_2 (Reference 22-34).

These metastable states will heat the electrons via superelastic collisions and consequently raise the nitrogen-vibrational temperature. This leads to a higher rate for the formation of NO^+ according to reaction (22-6) and hence faster removal (Reference 22-35) of electrons (Figure 22-1). The following metastable states play a similar role: $O(^1S)$, $N(^2P)$, $O^+(^2D)$, $O^+(^2P)$, $N^+(^1D)$, $N^+(^1S)$, $O_2(a^1\Delta)$, and $O_2(b^1\Sigma)$. However, one may neglect $O(^1S)$, $N(^2P)$, $O^+(^2P)$, $N^+(^1D)$, and $N^+(^1S)$ if the purpose of the code is the calculation of electron density. On the other hand, they cannot be ignored in optical and infrared calculations. $O^+(^2D)$ plays an important role since it resonantly charge-exchanges (Reference 22-36) with N_2:

$$O^+(^2D) + N_2 \rightarrow N_2^+(A^2\Pi) + O \quad , \tag{22-10}$$

and thereby changes an atomic ion into a molecular ion with a rate coefficient of $\sim(1 - 3) \times 10^{-9}$ cm^3 sec^{-1} (Reference 22-37).

To answer the question raised earlier on the accuracy of the electron density calculations, it may be concluded from the processes discussed above that one must include important metastable states or at least account for them in a realistic manner. In addition, the appropriate temperatures must also be calculated as functions of time.

22.3.2 Examples of Deionization Calculations in Disturbed E and F Regions

The Naval Research Laboratory (NRL) Master Deposition and Late Time Chemistry Code (References 22-38 through 22-40) (hereinafter referred to as the NRL Master Code) and The Simple Code (Reference 22-40) describe the deionization processes in disturbed E and F regions of the ionosphere. There are other deionization codes (References 22-41, 22-42) having varying degrees of complexity, with some similarity to the above codes. They carry many species and may be considered multispecies codes. Table 22-1 contains some important E and F region species which are carried by multispecies codes, especially by the NRL Master Code. Multispecies codes which calculate the electron temperature also consider additional excited states, which are short-lived and decay radiatively but are not carried individually. They are accounted for in the electron-temperature equation as cooling processes. Examples of these states are:

$$N_2^+(B^2\Sigma),\ N_2^+(A^2\Pi),\ N_2(c^3\Pi),\ N_2(B^3\Pi),\ \text{etc.}$$

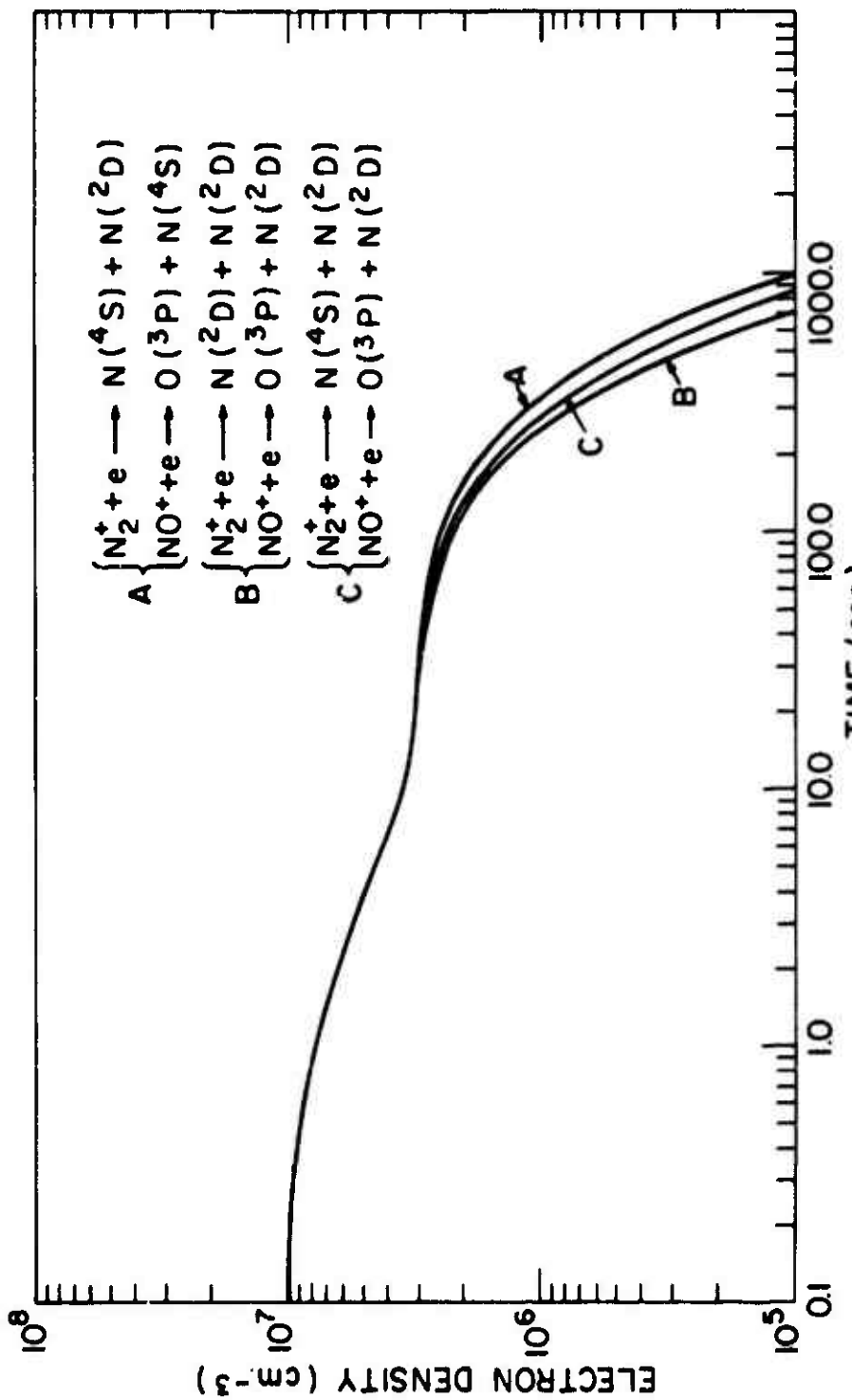

Figure 22-1. The effects of the products of two dissociative recombinations on electron density.

The significance of these and the states shown in Table 22-1 is obvious for the optical and infrared calculations.

Table 22-1. Some species of importance to E and F region multiple species computer codes.

Neutrals*	Neutral Excited States	Positive Ions	Positively Charged Excited States
N_2	$N_2(A^3\Sigma_u^+)$	N_2^+	
O	$\left\{\begin{matrix} O(^1D) \\ O(^1S) \end{matrix}\right.$	O^+	$\left\{\begin{matrix} O^+(^2D) \\ O^+(^2P) \end{matrix}\right.$
O_2	$\left\{\begin{matrix} O_2(a^1\Delta_g) \\ O_2(b^1\Sigma_g^+) \end{matrix}\right.$	O_2^+	$O_2^+(a^4\Pi_u)$
N	$\left\{\begin{matrix} N(^2D) \\ N(^2P) \end{matrix}\right.$	N^+	$\left\{\begin{matrix} N^+(^1D) \\ N^+(^1S) \end{matrix}\right.$
NO		NO^+	
$\left\{\begin{matrix} Me^{**} \\ MeO^{**} \end{matrix}\right.$		$\left\{\begin{matrix} Me^+ \\ MeO^+ \end{matrix}\right.$	

NOTES:

*One may include minor species such as CO_2, Ar, etc.

**Me denotes a metallic atom; MeO denotes a metallic oxide.

Some results of deionization calculations are shown in Figures 22-2 through 22-5. These results are taken from the calculations of Lewis and Ali (Reference 22-43) who have utilized the NRL Master Code. In these calculations the nitrogen-vibrational temperature (Reference 22-40) is computed assuming a harmonic oscillator model (Reference 22-44). However, one may calculate (References 22-38 through 22-40) the time histories of the individual vibrational levels instead of a vibrational temperature. Of course, this adds to the complexity of the code. The reason for carrying individual vibrational states lies in the fact that each vibrational state of N_2 has a different reaction rate for the formation of NO^+ (Reaction 22-6). For example, the $v = 4$ state has a rate coefficient which is at least two orders of magnitude larger (Reference 22-29) than the $v = 1$ or $v = 0$ state. Figure 22-6 shows a deionization calculation where the time histories of the vibrational levels are indicated.

Some remarks concerning the results in Figures 22-2 through 22-5 are in order: Figures 22-2 and 22-3 show the deionization calculations for a given initial condition at an altitude of 200 km where densities of N_2, O, and O_2 are 3.25×10^9, 3.216×10^9, and 3.5×10^8 cm^{-3}, respectively. No molecular ions are present because of the complete ionization of the region. The electron density decreases by a factor of 2 over ~300 seconds due to radiative recombination resulting in an increase in the N and O concentrations. An interesting picture, however, appears for a lower degree of ionization at the same altitude (Figures 22-4 and 22-5). In this case the degree of ionization is ~12 percent. N_2^+ and O_2^+ are depleted within ~10 seconds (Figure 22-4). NO^+ is abundant and is mainly responsible for the removal of the electrons for times beyond a few seconds. The electron density decreases by ~3 orders of magnitude over a period of 300 seconds because of the presence of molecular ions (cf. the initial case). The increase in the neutral particle densities arises from dissociative recombination. The early time increase in the metastable neutral particle concentrations is due to direct electron impact excitation and the dissociative recombinations.

It is obvious that such a multispecies treatment cannot, at least at this time, be carried in three-dimensional magnetohydrodynamic codes. However, if the purpose of the deionization calculations is determination of the electron density, then one may use the Simple Chemistry Code (Reference 22-40) and eliminate most of the metastable states by accounting realistically for their effects on the

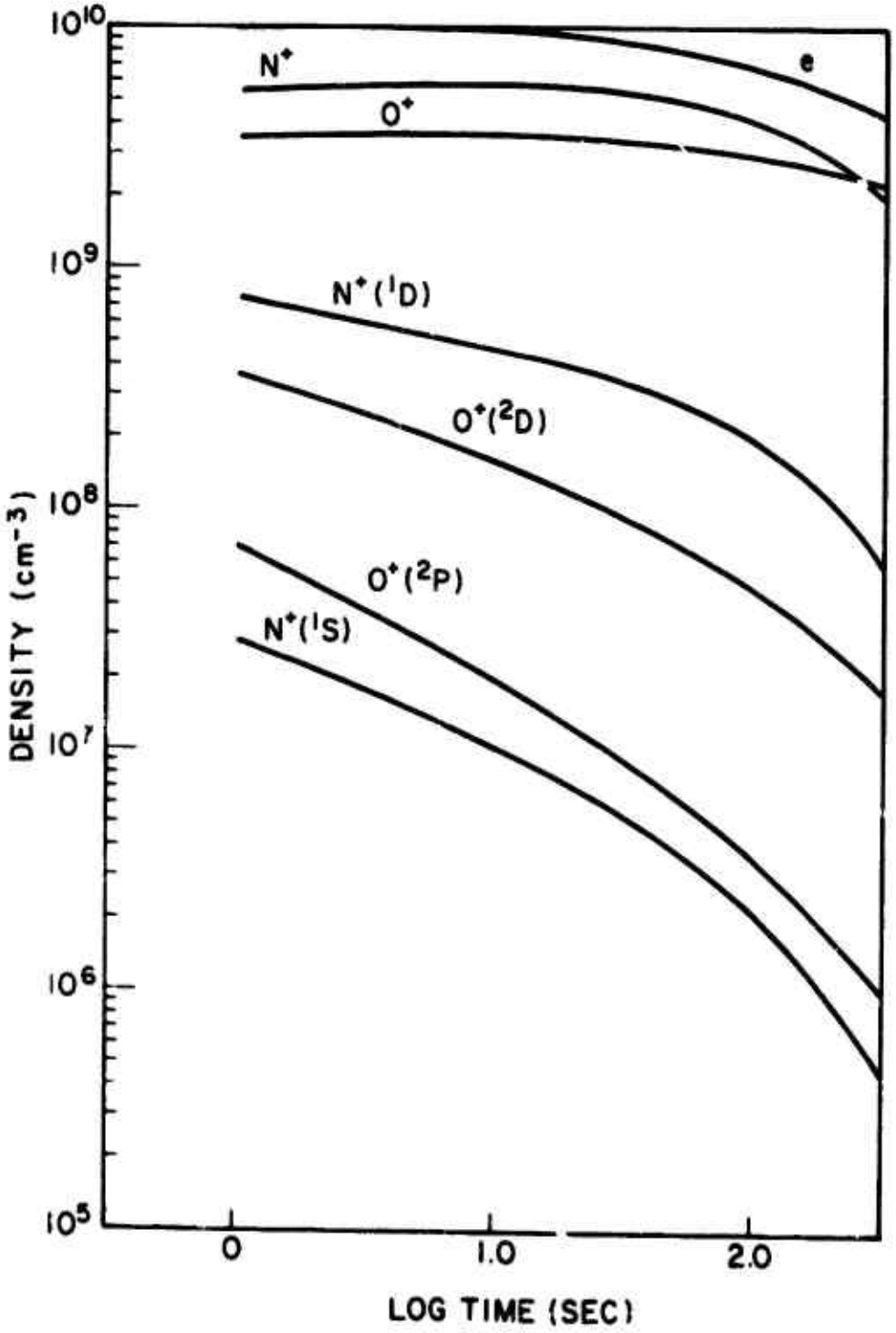

Figure 22-2. Electran and atomic-ion densities for a given initial conditian at 200 km altitude.

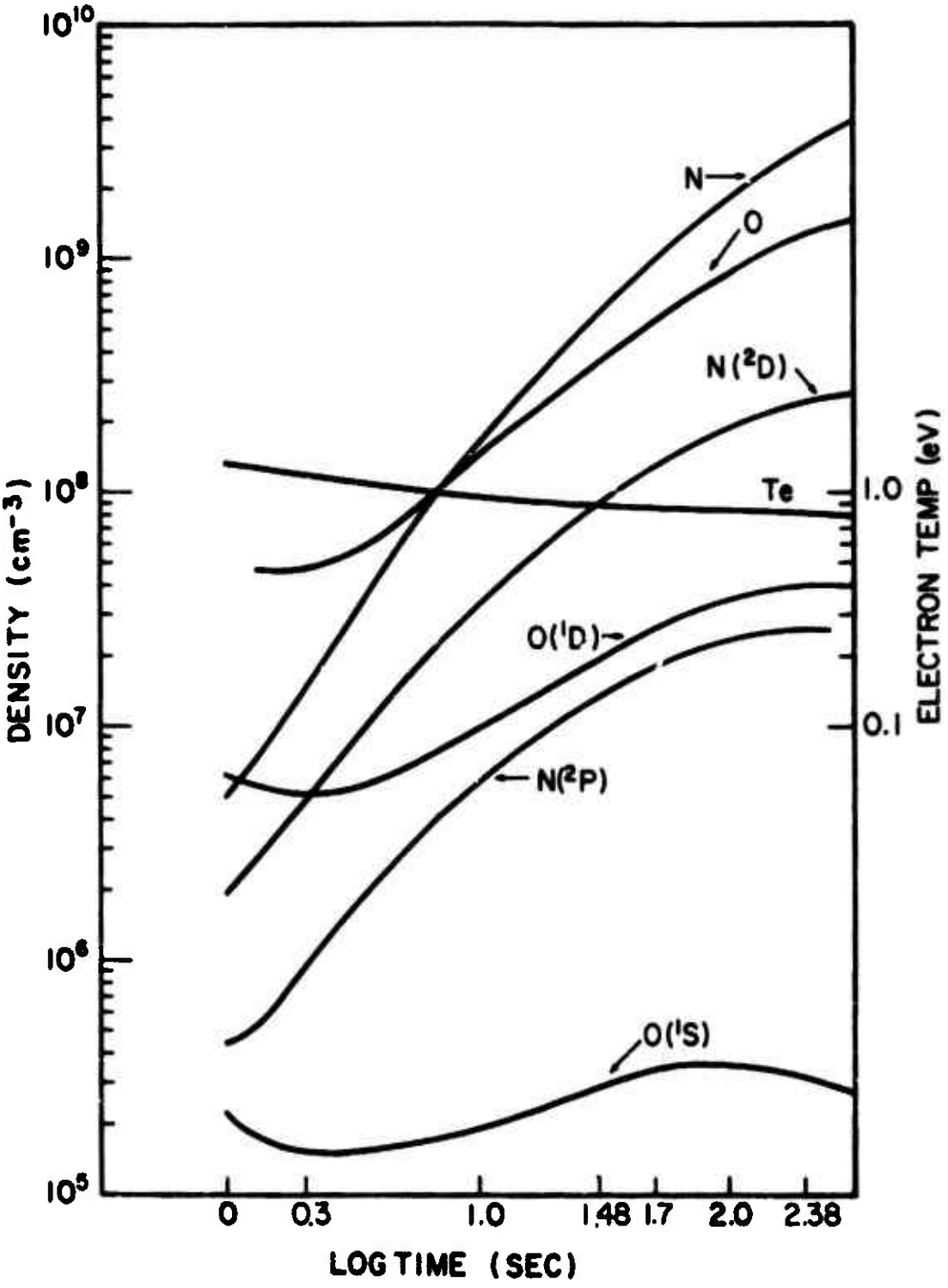

Figure 22-3. Other species densities for the same point as in Figure 22-2.

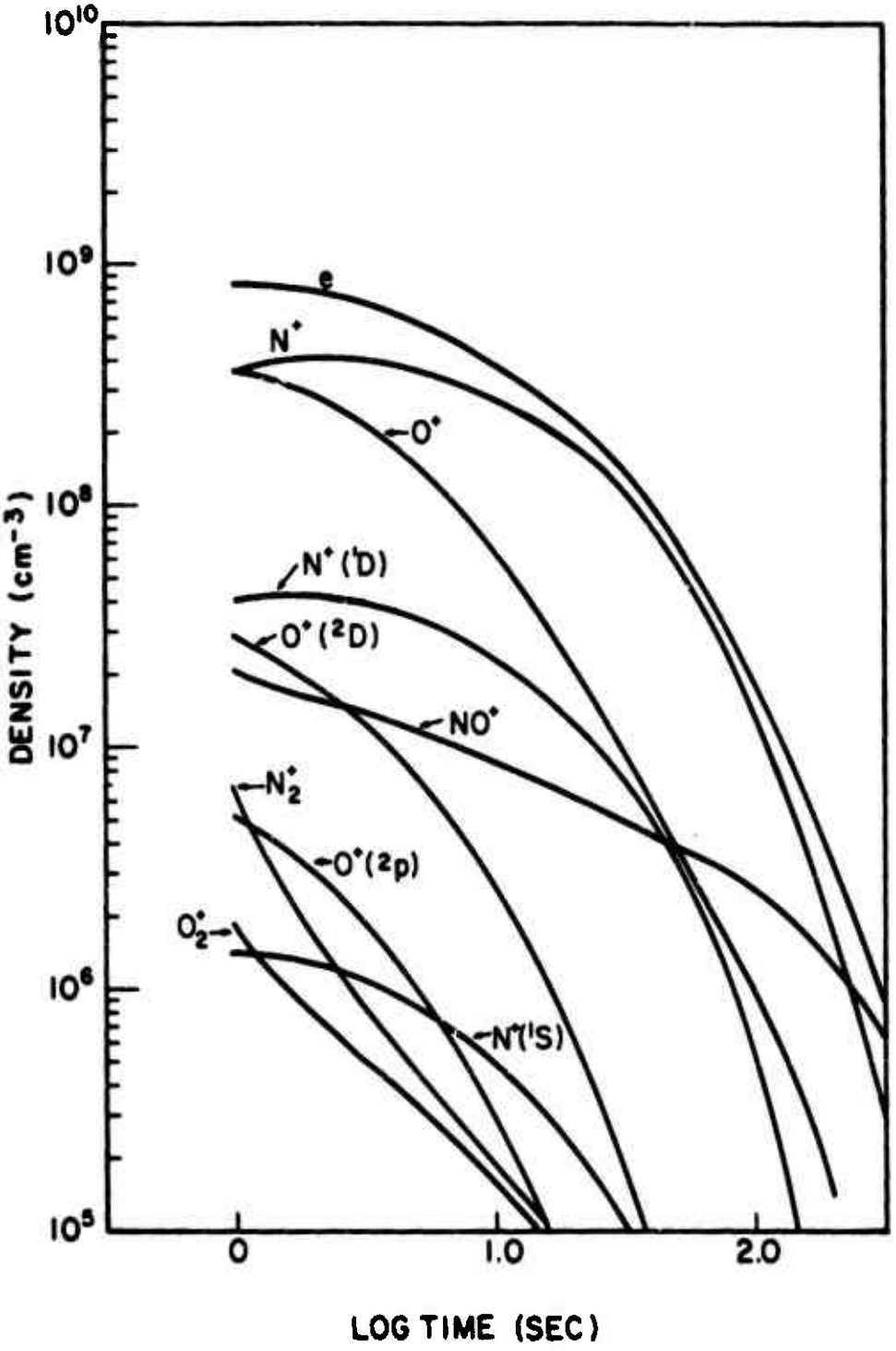

Figure 22-4. Electron and ion densities ot the same altitude but for a lower degree of ionization compared with Figure 22-2.

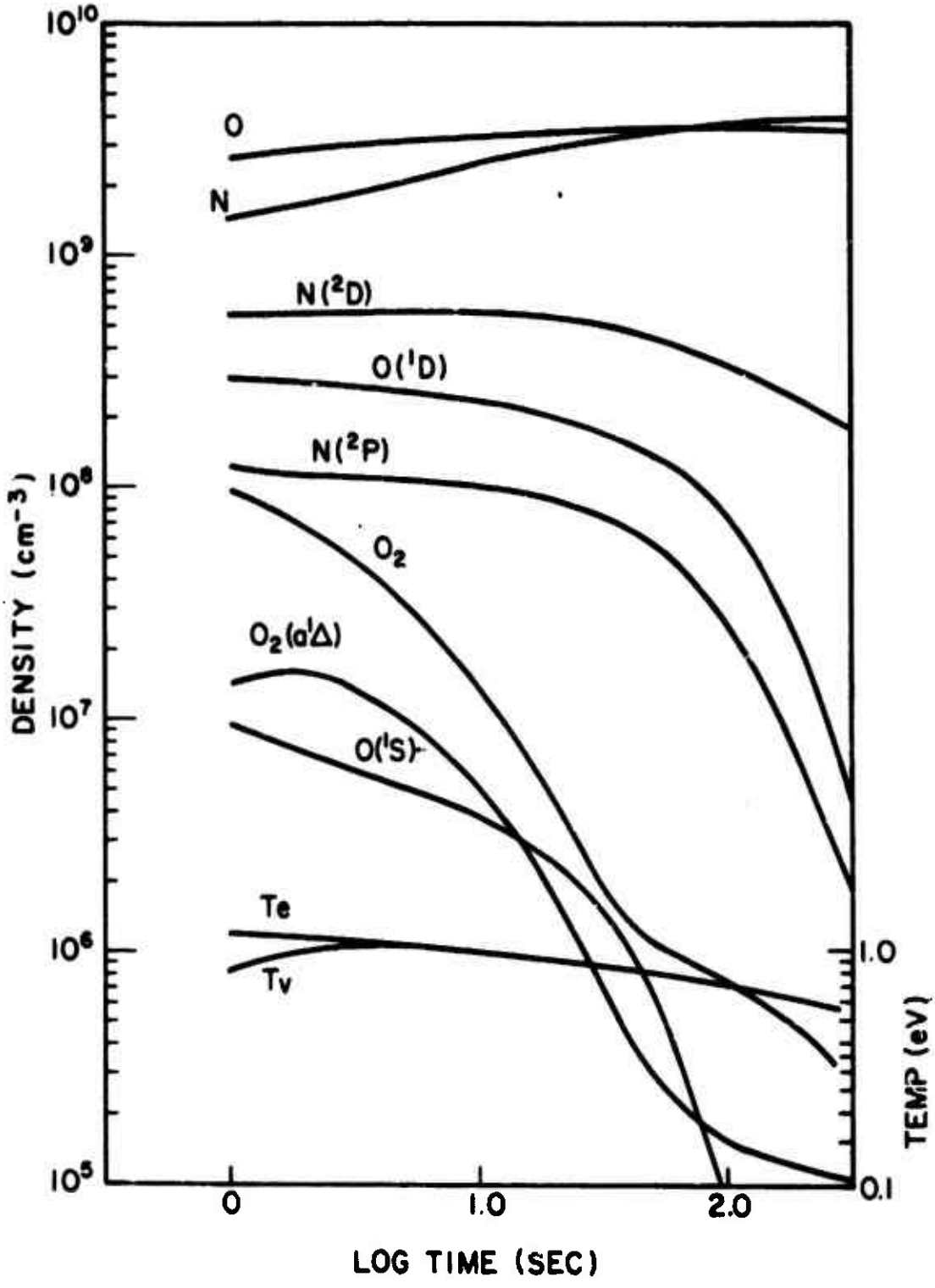

Figure 22-5. Other species densities for the same point as in Figure 22-4.

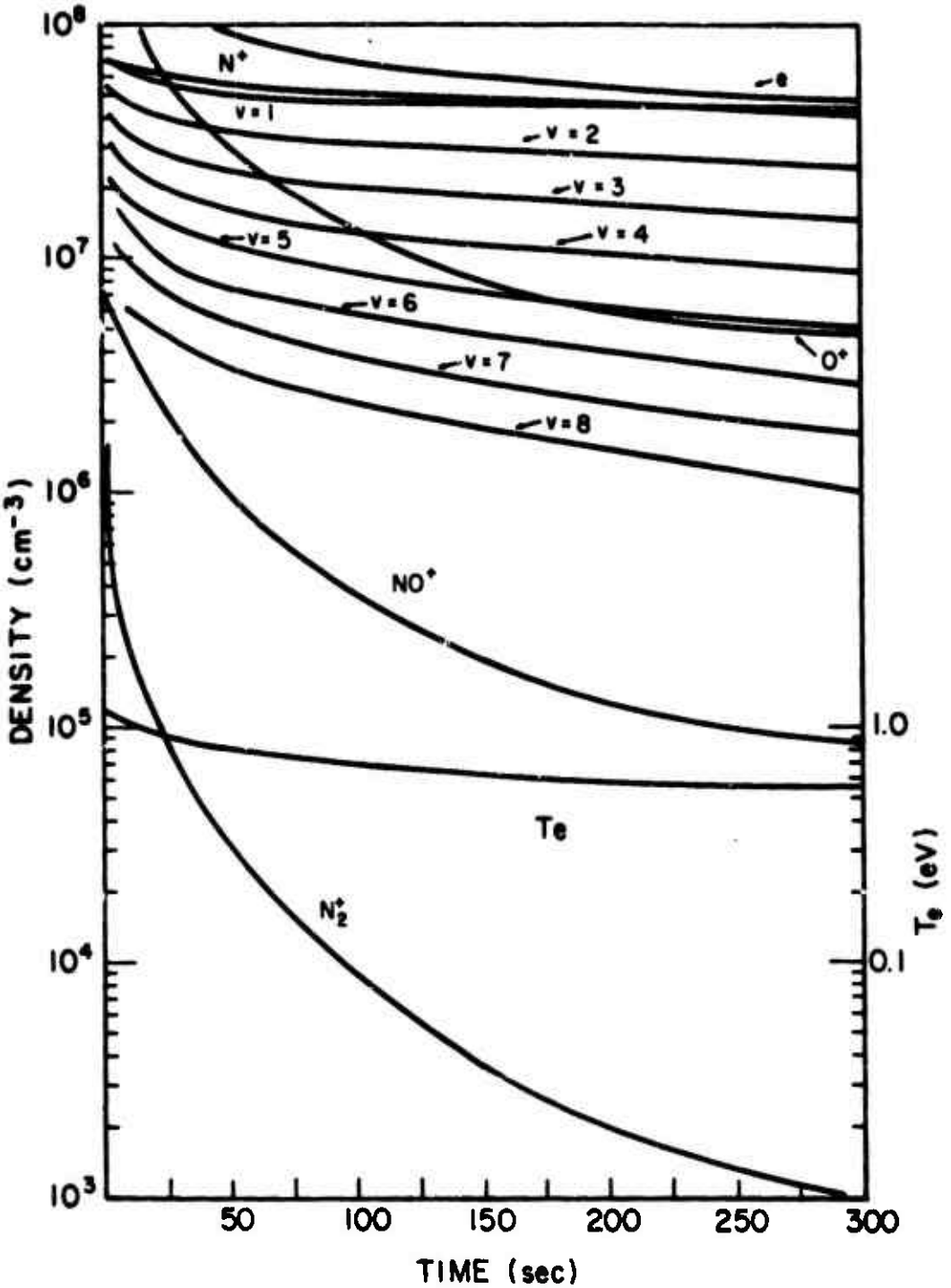

Figure 22-6. Deionization calculations with varying vibrational state of nitrogen.

deionization process. Figures 22-7 and 22-8 show a comparison between the electron density as calculated by the Simple Code (smooth curves) and the NRL Master Code (XXX and OOO) for six different ionization cases. As an example, Figure 22-9 shows a comparison between some ionic species densities, for a given case (Case I of Figure 22-7) as calculated by both codes.

From these examples one may infer that simplification in the chemistry is possible. However, if one is interested in the optical and infrared emission, simplification can hardly be justified.

22.3.3 The Disturbed D-Region Multispecies Codes

The D-region chemistry is more complex than that of the E and F regions, because:

(a) The D region is denser, which enhances the occurrence of three-body processes, especially the three-body attachment of electrons to O_2.

(b) The D region has many more minor species (see Table 22-2) which play an important role in ion-cluster formation.

The deionization processes discussed in Section 22.3.1, e.g., dissociative recombination, ion-molecule interaction, and charge exchange, which are responsible for the removal of electrons in the E and F regions are equally valid in the D region. However, several different physical processes arise in the D region. The three-body attachment of the electron to O_2 according to the reaction:

$$e + O_2 + M \rightarrow O_2^- + M \qquad (22\text{-}11)$$

becomes an important electron removal process and has a rate coefficient (Reference 22-45) of $\sim 10^{-30}$ cm^6 sec^{-1} at D-region temperature. Reaction (22-11), the charge exchange:

$$O_2^- + O_3 \rightarrow O_3^- + O_2 \quad , \qquad (22\text{-}12)$$

and the dissociative attachment to O_3 start the negative-ion reaction sequence. Figure 22-10 shows a schematic diagram (Reference 22-46) for the formation of negative-ion clusters through many possible reactions of the negative ions with H_2O, CO_2, and NO_2.

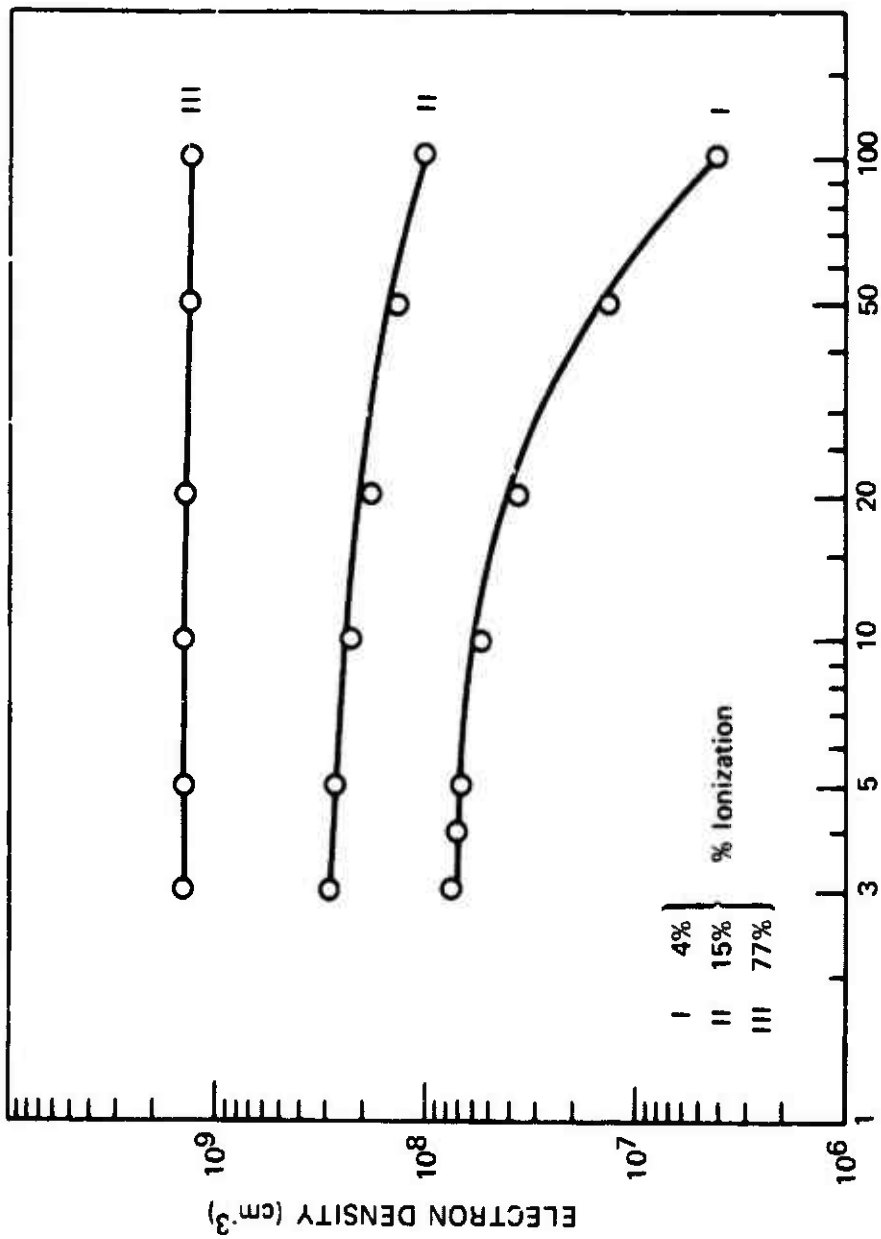

Figure 22-7. Comparison of electron density calculations (smooth curve, NRL Simple Code; OOO, NRL Master Code).

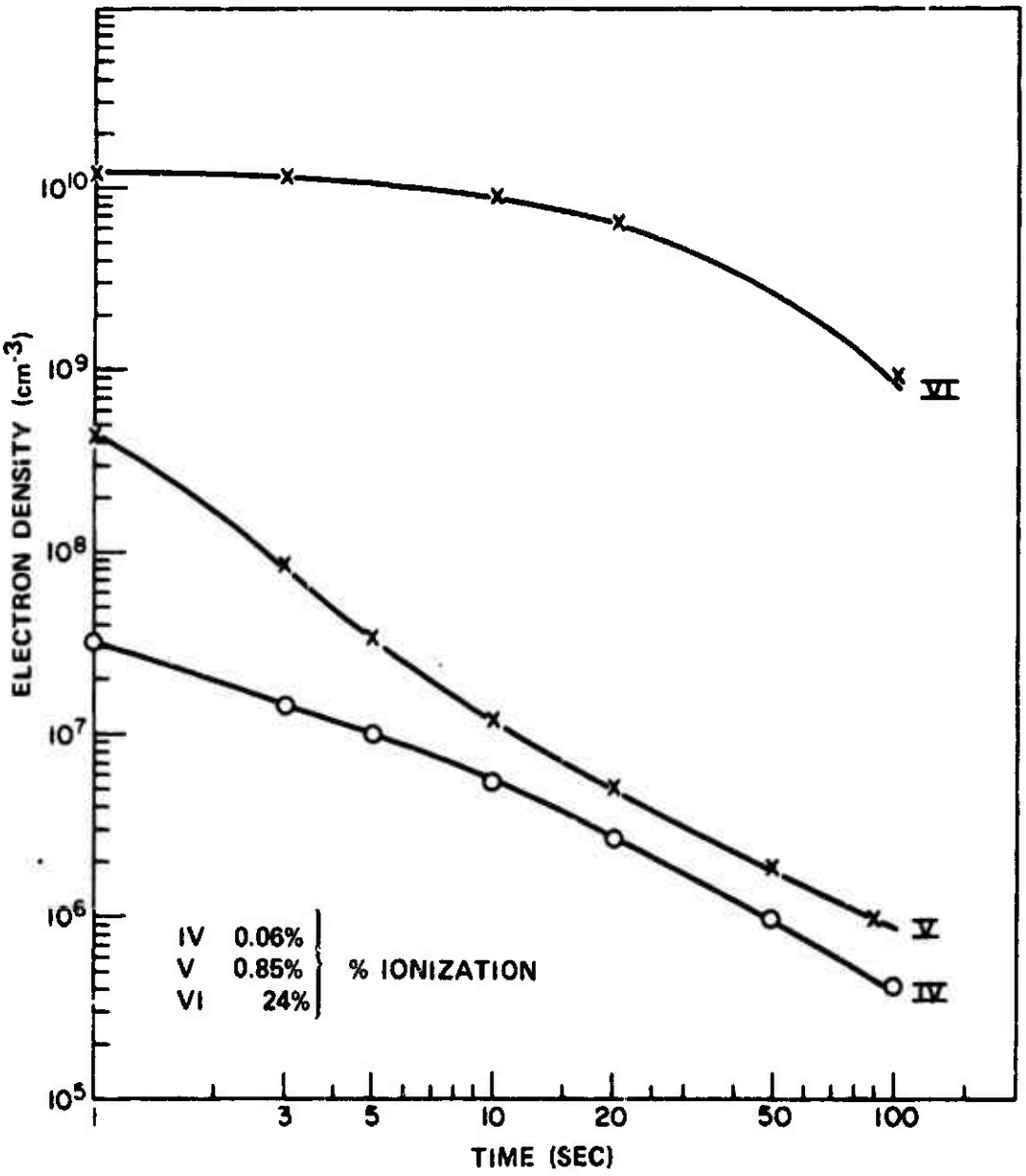

Figure 22-8. Comparison of the electron density calculations (smooth curve, NRL Simple Code; XX OO, NRL Master Code).

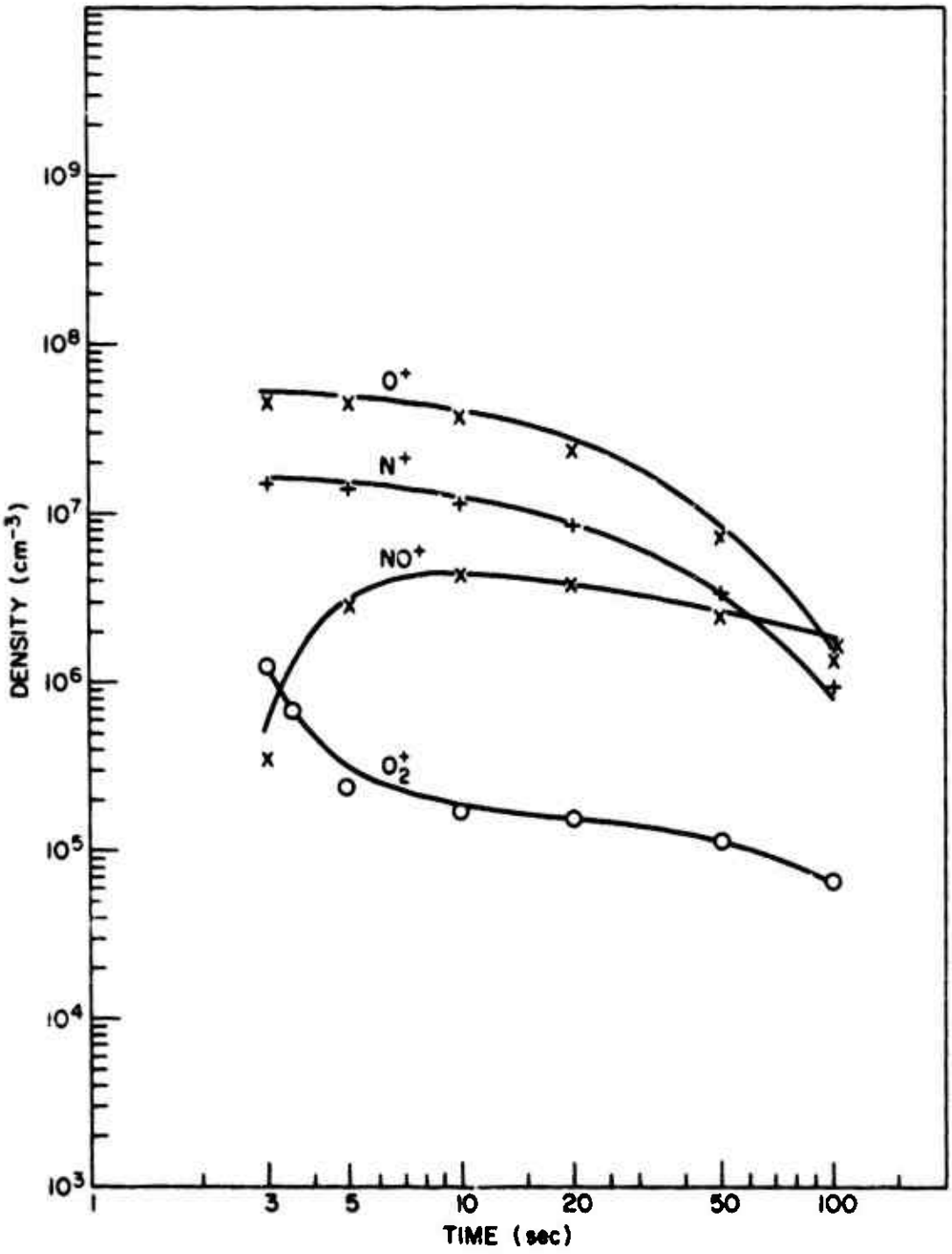

Figure 22-9. Comparison of ion density calculations for Case I of Figure 22-7 (smooth curves, NRL Simple Code; XX 00, NRL Master Code).

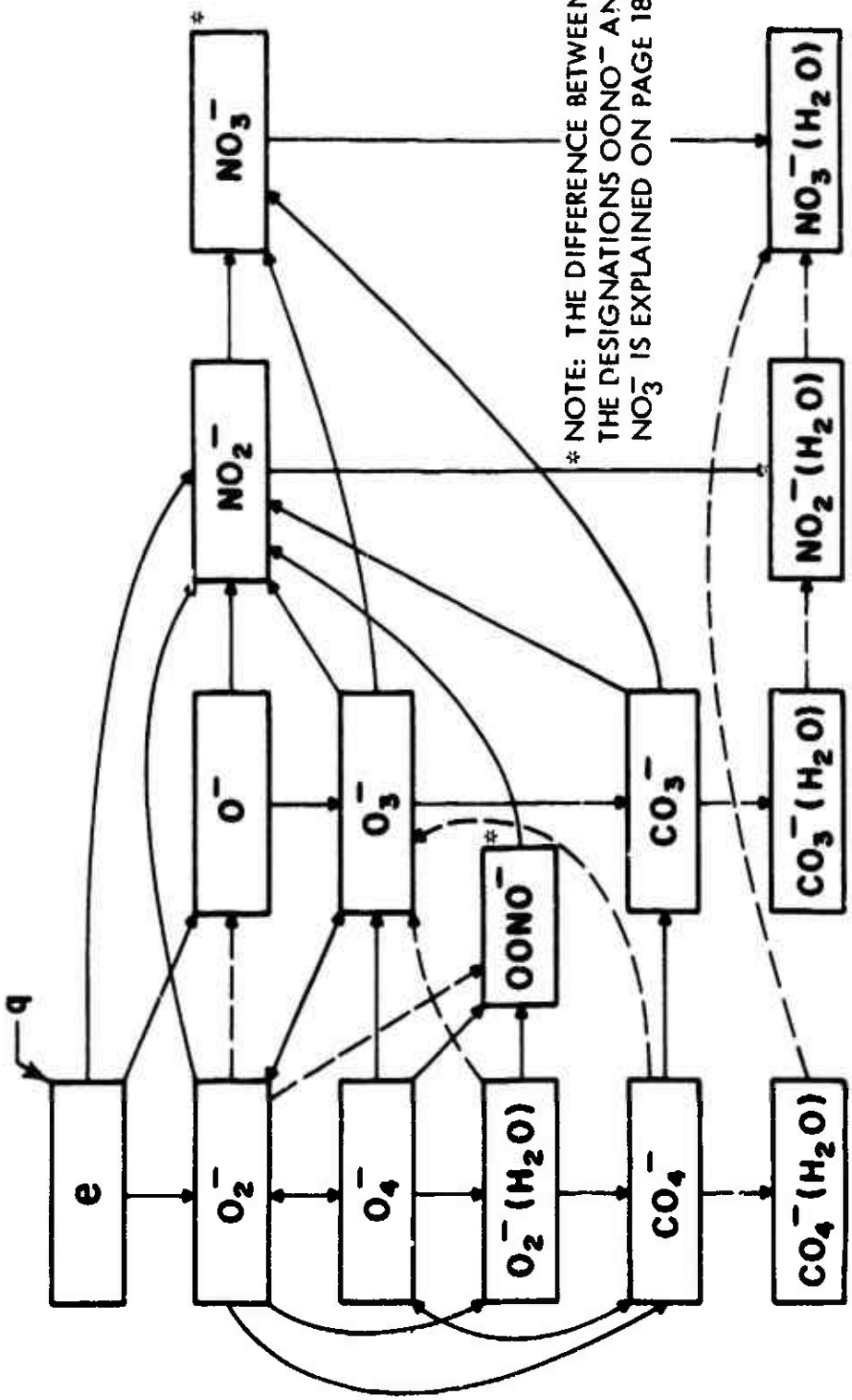

Figure 22-10. Schemotic representation of the formation of negative ions in ionized air. The solid lines indicate probable reactions, on the basis of experimental measurements of the rate coefficients.

Table 22-2. Some species of importonce to the Sub-D- ond D-regions multispecies computer codes.

Neutrals	Neutral Excited States	Negatives	Positives
CH_4	$N(^2D)$	CO_3^-	$H^+(H_2O)_{n=1-5}$
CO	$N_2(A^3\Sigma_u^+)$	$CO_3^-(H_2O)$	$H^+(H_2O)(HO)$
CO_2	$O(^1D)$	CO_4^-	$H^+(H_2O)(N_2)$
H	$O(^1S)$	$CO_4^-(H_2O)$	N^+
HNO_2	$O_2(a^1\Delta_g)$	NO_2^-	NO^+
HNO_3	$O_2(b^1\Sigma_g^+)$	$NO_2^-(H_2O)$	$NO^+(CO_2)$
HO		NO_3^- *	$NO^+(H_2O)_{n=1-3}$
HO_2		$NO_3^-(H_2O)_{n=1-5}$	$NO^+(N_2)$
H_2		O^-	NO_2^+
H_2O		O_2^-	N_2^+
H_2O_2		$O_2^-(H_2O)$	O^+
N		O_3^-	O_2^+
NO		O_4^-	$O_2^+(H_2O)$
NO_2		$OONO^-$ *	O_4^+
NO_3		e	
N_2			
N_2O			
N_2O_5			
O			
O_2			
O_3			

*The difference between the designations $OONO^-$ and NO_3^- is explained on page 18A-7.

The formation of positive-ion clusters, on the other hand, starts with the formation of O_4^+ according to:

$$O_2^+ + O_2 + M \rightarrow O_4^+ + M \quad , \tag{22-13}$$

which in turn reacts with H_2O:

$$O_4^+ + H_2O \rightarrow O_2^+(H_2O) + O_2 \quad , \tag{22-14}$$

to produce the singly hydrated molecular oxygen ion.

A detailed scheme shown in Figure 22-1' indicates the possible mechanisms for the formation of positive-ion clusters (Reference 22-46).

22.3.4 Exomples of D-Region Deionizotion Colculotions

Niles (References 22-46 and 22-47), and Scheibe (Reference 22-48) have developed disturbed D-region deionization codes which are multispecies with hundreds of reactions. These codes have been used to carry out several deionization calculations (References 22-46 through 22-51) for the beta patch and cool D region outside the fireball. These calculations have not included transport. This was the case also for the E- and F-region calculations presented earlier. However, codes are being developed which include transport and a limited number of reactions (Reference 22-52). Since for most of the species in the D region the time constant for reaction is much less than the time constant for diffusion, the omission of transport should not greatly affect atmospheric deionization. However, this is not true for the E and F regions.

The calculations of the multispecies codes presented here are for the 60-km region, where UHF attenuation is greatest (Reference 22-46). These calculations utilize the model atmosphere given in Table 22-3 and the analytic expressions in Table 22-4 for the electron productions produced by beta-ray ionization.

A composite of the electron-density decays (Reference 22-46) in the beta patch at an altitude of 150 km is given in Figure 22-12. The decay curves are identified by the altitude (in kilometers) to which the curve applies. The form of the electron-density decay divides readily into two temporal regions. The electrons created

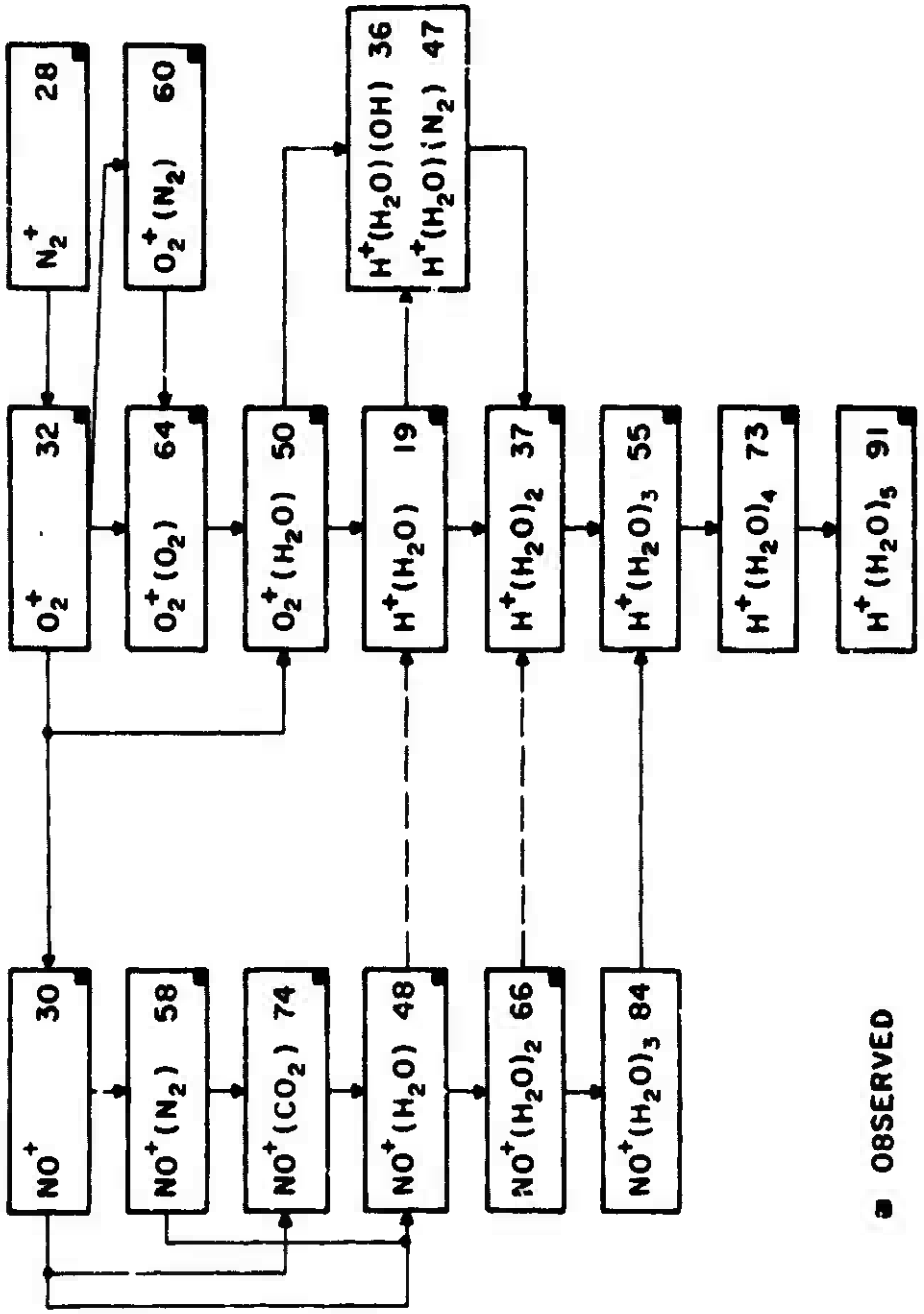

Figure 22-11. Schematic representation of the formation of positive ions in the D region. The solid lines indicate known reactions. The dashed lines indicate possible reactions.

Table 22-3. Model atmosphere far beta-patch calculations.

Altitude (km)	50	55	60	65	70	75	80
Temperature (K)	271.0	257.2	243.3	230.0	216.6	201.3	186.0
Total Density (cm^{-3})	2.15(16)	1.20(16)	6.60(15)	3.42(15)	1.76(15)	8.31(14)	3.81(14)
N_2(cm^{-3})	1.70(16)	9.6 (15)	5.2 (15)	2.7 (15)	1.4 (15)	6.6 (14)	3.0 (14)
O_2	4.5 (15)	2.4 (15)	1.4 (15)	7.2 (14)	3.6 (14)	1.7 (14)	8.0 (13)
CO_2	9.7 (12)	4.5 (12)	2.5 (12)	1.2 (12)	5.2 (11)	1.2 (11)	1.0 (11)
H_2O	8.2 (10)	4.0 (10)	2.2 (10)	1.0 (10)	4.0 (9)	7.5 (8)	3.2 (7)
N	3.3 (6)	1.8 (6)	1.0 (6)	–	–	–	–
NO	6.0 (9)	4.0 (9)	2.0 (9)	1.3 (9)	7.0 (8)	4.5 (8)	2.0 (8)
N_2O	1.4 (10)	9.0 (9)	3.6 (9)	2.3 (9)	9.5 (8)	6.0 (8)	2.5 (8)
NO_2	5.5 (5)	3.1 (5)	1.7 (5)	5.5 (3)	9.1 (3)	6.0 (3)	3.5 (3)
NO_3	5.5 (2)	3.1 (2)	1.7 (2)	4.0 (1)	1.0 (1)	2.5	–
O	9.7 (9)	1.2 (10)	1.5 (10)	2.2 (10)	2.8 (10)	6.5 (10)	1.0 (11)
O_3	6.0 (10)	3.4 (10)	8.0 (9)	5.0 (9)	1.5 (9)	1.3 (9)	1.2 (8)
$O_2(^1\Delta)$	5.0 (10)	3.0 (10)	2.0 (10)	1.4 (10)	8.0 (9)	4.5 (9)	3.2 (9)
e	2.0 (10)	4.0 (10)	7.0 (10)	1.5 (11)	2.0 (11)	3.0 (11)	4.0 (11)
N_2^+	1.6 (10)	3.2 (10)	5.6 (10)	1.2 (11)	1.6 (11)	2.4 (11)	3.2 (11)
O_2^+	3.2 (9)	6.4 (9)	1.1 (10)	2.4 (10)	3.2 (10)	4.8 (10)	6.4 (10)
O	8.0 (8)	1.6 (9)	2.8 (9)	6.0 (9)	8.0 (9)	1.2 (10)	1.6 (10)

N.B.: Numbers given in the form m(n) correspond to $m \cdot 10^n$.

Table 22-4. Analytical expressions for electron production [$q(e,t) = f(t)\ cm^{-3}\ sec^{-1}$].

Altitude (km)	f(t) (t in sec)
80	$4.7 \times 10^{7}(1+t)^{-1.2}(1+15\,e^{-t/20})$
75	$9.3 \times 10^{7}(1+t)^{-1.2}(1+12\,e^{-t/20})$
70	$1.4 \times 10^{8}(1+t)^{-1.2}(1+9\,e^{-t/20})$
65	$1.6 \times 10^{8}(1+t)^{-1.2}(1+12\,e^{-t/20})$
60	$1.8 \times 10^{8}(1+t)^{-1.2}(1+15\,e^{-t/20})$
55	$1.6 \times 10^{8}(1+t)^{-1.2}(1+12\,e^{-t/20})$
50	$1.4 \times 10^{8}(1+t)^{-1.2}(1+9\,e^{-t/20})$

by prompt radiation decay initially by dissociative recombination with N_2^+ and then with O_2^+ in Region I. Region II begins when the electron density is affected by the ionization produced by the beta rays. In Region II, the electron density is lost primarily by dissociative recombination with NO^+ in the upper part of the beta patch and by electron attachment to O_2 in the lower part. In agreement with this, the dependence of the electron density on the source term, q(e,t), changes from square root in the upper part to linear in the lower part. In between, the electron density decay is complex.

In Region I, the decay of electron density is given by:

$$dn_e/dt = \alpha_d n_e n_+ \quad , \tag{22-15}$$

where n_+ is the total positive-ion density and α_d is the lumped dissociative-recombination coefficient. Since $n_e \approx n_+$, the solution can be written as:

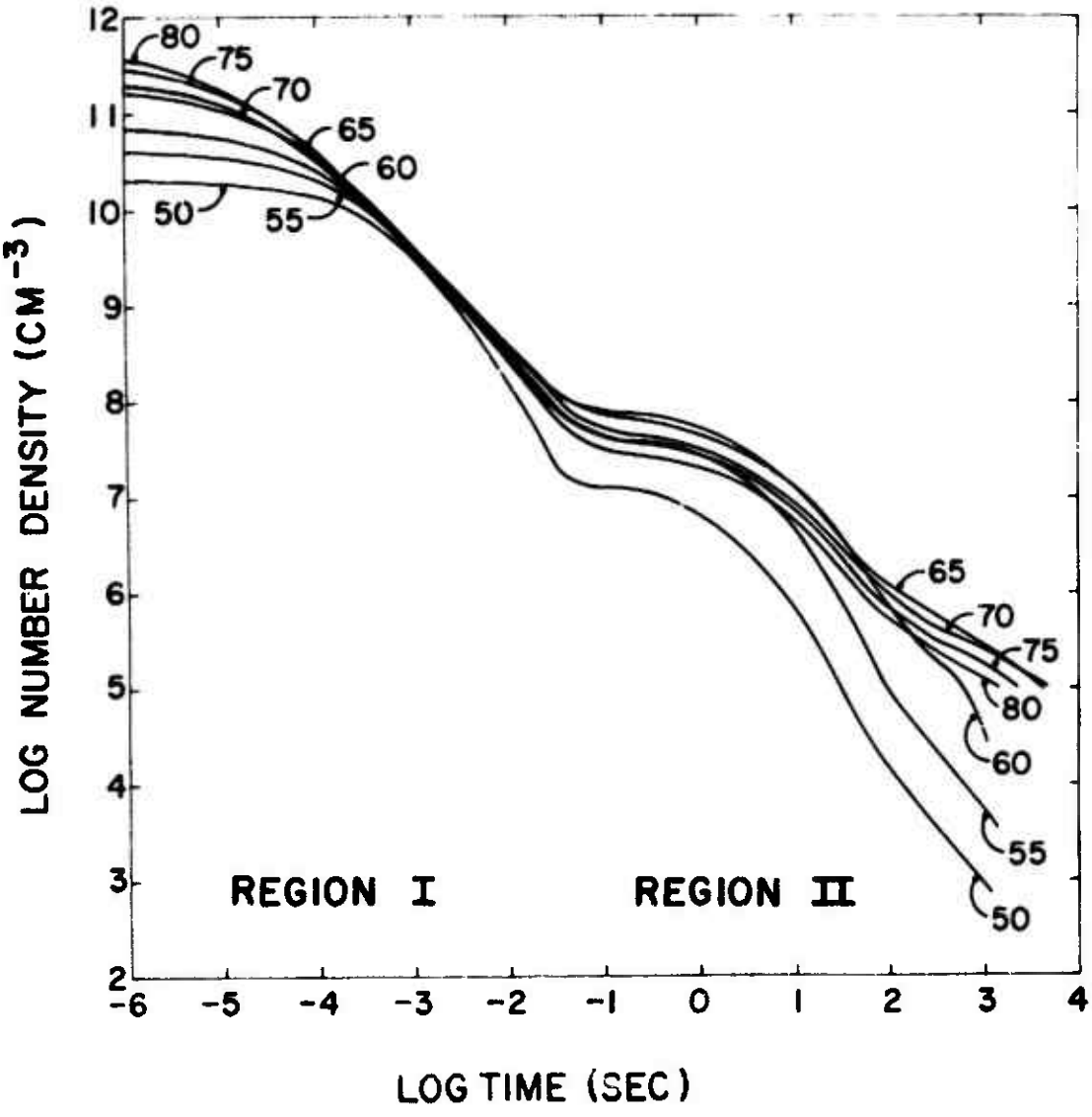

Figure 22-12. Decay of electran density in the beta patch at 150 km altitude. The numbers associated with the decay curves give the altitude in kilometers (Reference 22-46).

$$n_e = (n_e)_0/[(1 + (n_e)_0 \alpha_d t] \quad , \tag{22-16}$$

where $(n_e)_0$ is the initial electron density immediately after the burst.

Since the dissociative-recombination rate constants for N_2^+ and O_2^+ recombining with electrons are about 3×10^{-7} cm^3 sec^{-1} and the initial electron density is about 10^{11} cm^{-3}, Equation (22-16) reduces, at $t > 10^{-4}$ sec, to:

$$n_e = 1/\alpha_d t \quad . \tag{22-17}$$

This says that if there were no source term and if chemistry were unimportant, then the electron-density decay would be the same for all altitudes and all levels of initial ionization in the beta patch. Figure 22-12 shows a temporal region between 10^{-4} and 10^{-2} sec which corresponds to this situation, within which the time required for the electron density to decay to a specified value apparently could be readily determined. However, as seen in Figure 22-12, this is not the case.

In Region II, the decay of electron density in the upper part of the beta patch is given by:

$$dn_e/dt = q(e,t) - \alpha_d n_e n_+ \quad . \tag{22-18}$$

The quasi-equilibrium solution when $n_e = n_+$ is:

$$n_e = [q(e,t)/\alpha_d]^{0.5} \quad . \tag{22-19}$$

In the lower part of the beta patch the decay of electron density is given by:

$$dn_e/dt = q(e,t) - An_e \quad , \tag{22-20}$$

where A is the electron attachment frequency. Since A is determined primarily by three-body attachment of O_2 and since the O_2 density is nearly time-invariant, the quasi-equilibrium solution is:

$$n_e = q(e,t)/A \quad . \tag{22-21}$$

The relative importance of the various reactions which affect the electron density changes with time. The rates for the populating reactions at 60 km are shown in Figure 22-13, where Reactions 1, 15, and 201 denote, respectively, photodetachment, associative detachment, and collisional de-excitation detachment reactions of O_2^-. The depopulating reactions for the electron density giving rise to atmospheric deionization are shown in Figure 22-14 along with their rates. It is seen that dissociative recombination, first with N_2^+ and then with O_2^+, is the dominant loss process out to about 10 sec, at which time three-body attachment to O_2 becomes dominant.

The importance of cluster ions can be deduced from the rates for Reactions 296, 327, and 334 (Figure 22-14). These represent, respectively, the dissociative recombinations of O_4^+, $H_3O^+(H_2O)$, and $H_3O^+(H_2O)_2$ with electrons. Since for this altitude the initial conditions for the calculations assumed the ambient densities of these ions to be zero, the increase in rates reflects the rapid growth in cluster-ion densities.

Figures 22-15 through 22-17 show the results (Reference 22-46) of a deionization calculation for a beta patch at 60 km. The figures show the negative ions, the positive ions, and the neutral densities, respectively.

Scheibe (Reference 22-53) has produced a simplified analytic model for the disturbed D-region chemistry by obtaining analytical approximations for the species densities. His approach is based on the fact that for a moderate to high-level ionization without appreciable heating, a sudden ionization phenomenon can be separated into four distinct regions in time. The first period comprises the ionization, dissociation, and excitation of the air by x-rays, and is over in a very short time. The second phase includes recombination, charge-exchange, and ion-neutral reactions producing NO, O, and N. Even though the time scale for phase two is long compared to phase one, it is usually complete in $\sim$1 sec. At this stage the charged-particle chemistry is no longer coupled to the neutrals chemistry. The third phase involves the decay of O, N, $O_2(a^1\Delta)$, and NO and the production of O_3 and NO_2. The final phase is the late-time deionization whose solution is based on the fact that after a short time the charged-particle concentrations will achieve a steady-state condition and the concentrations can be obtained by algebraic relations. However, this may not always be true for such species as NO^+, NO_3^-, CO_3^-, and e. For these species one could solve the appropriate rate equations.

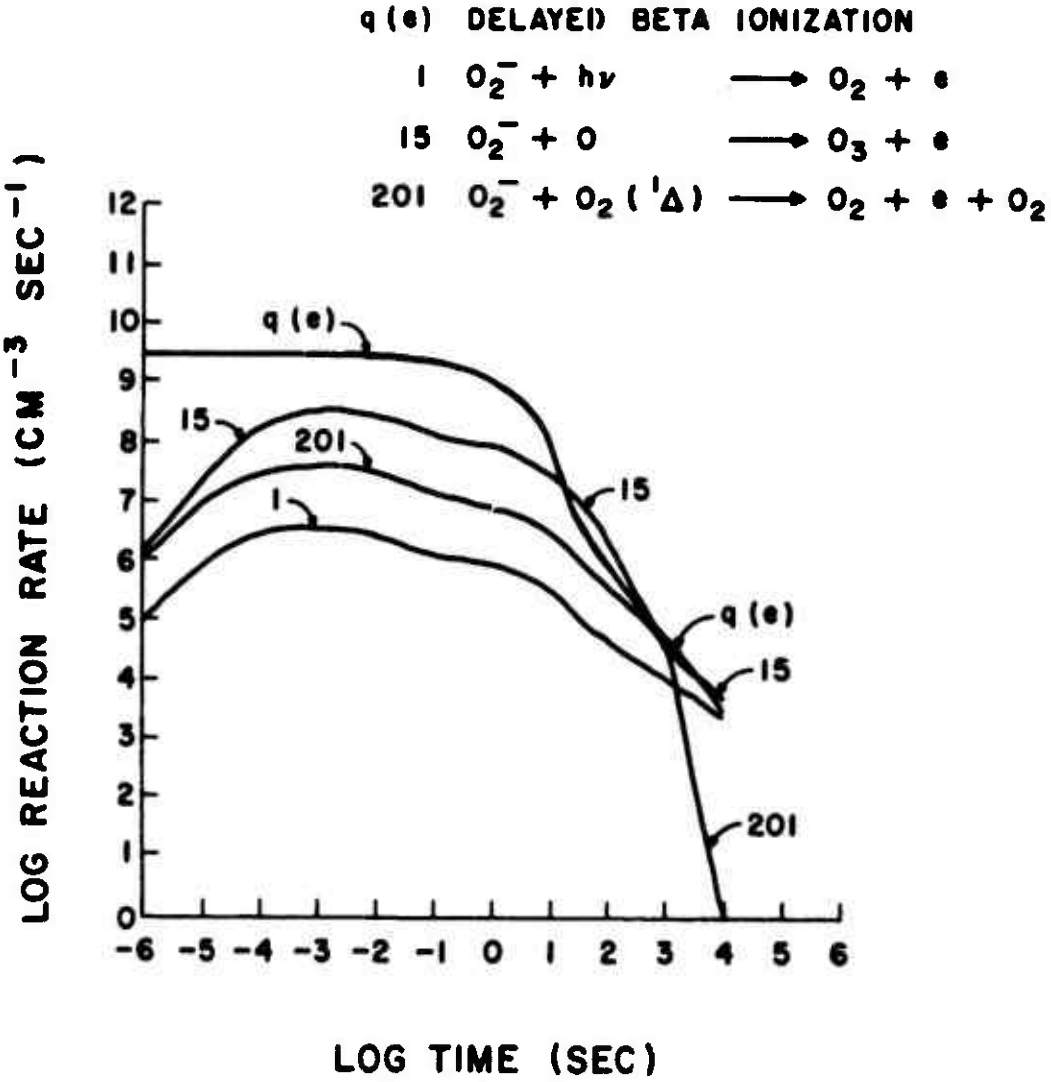

Figure 22-13. Electron populating rates at 60 km altitude in the beta patch (Reference 22-46).

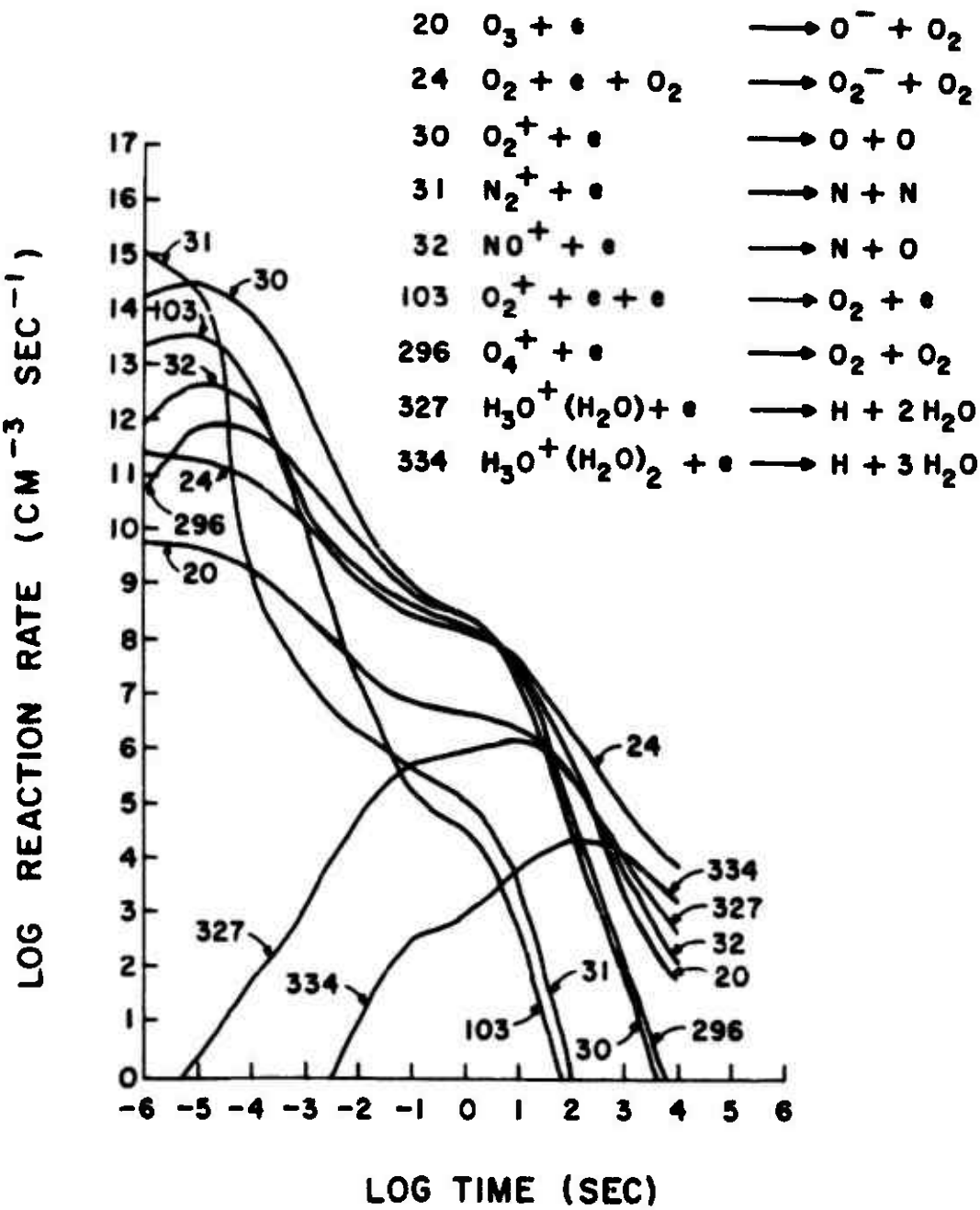

Figure 22-14. Electron depopulating rates at 60 km altitude in the beta patch (Reference 22-46).

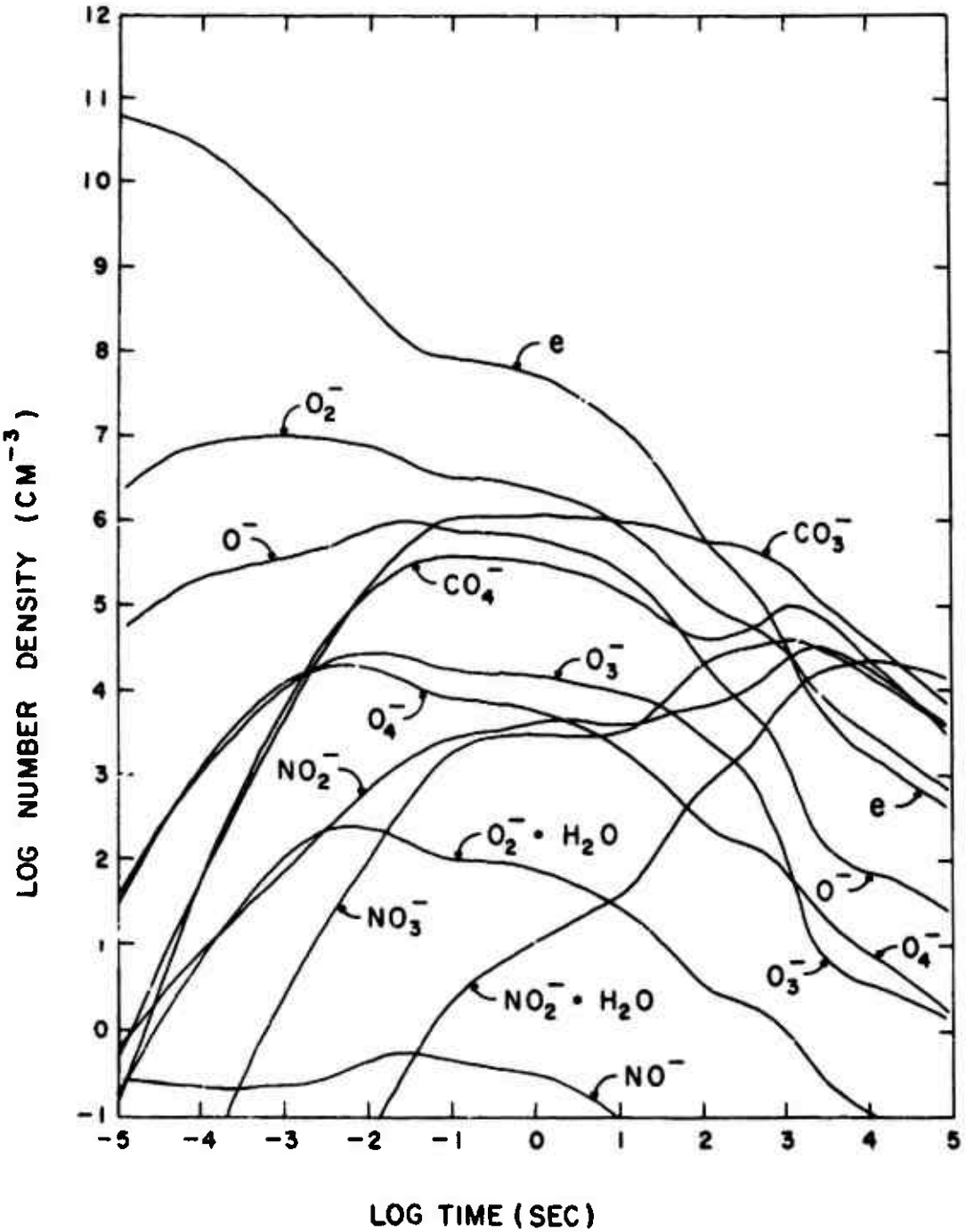

Figure 22-15. Electron and negative-ion densities at 60 km altitude in the beta patch (Reference 22-46).

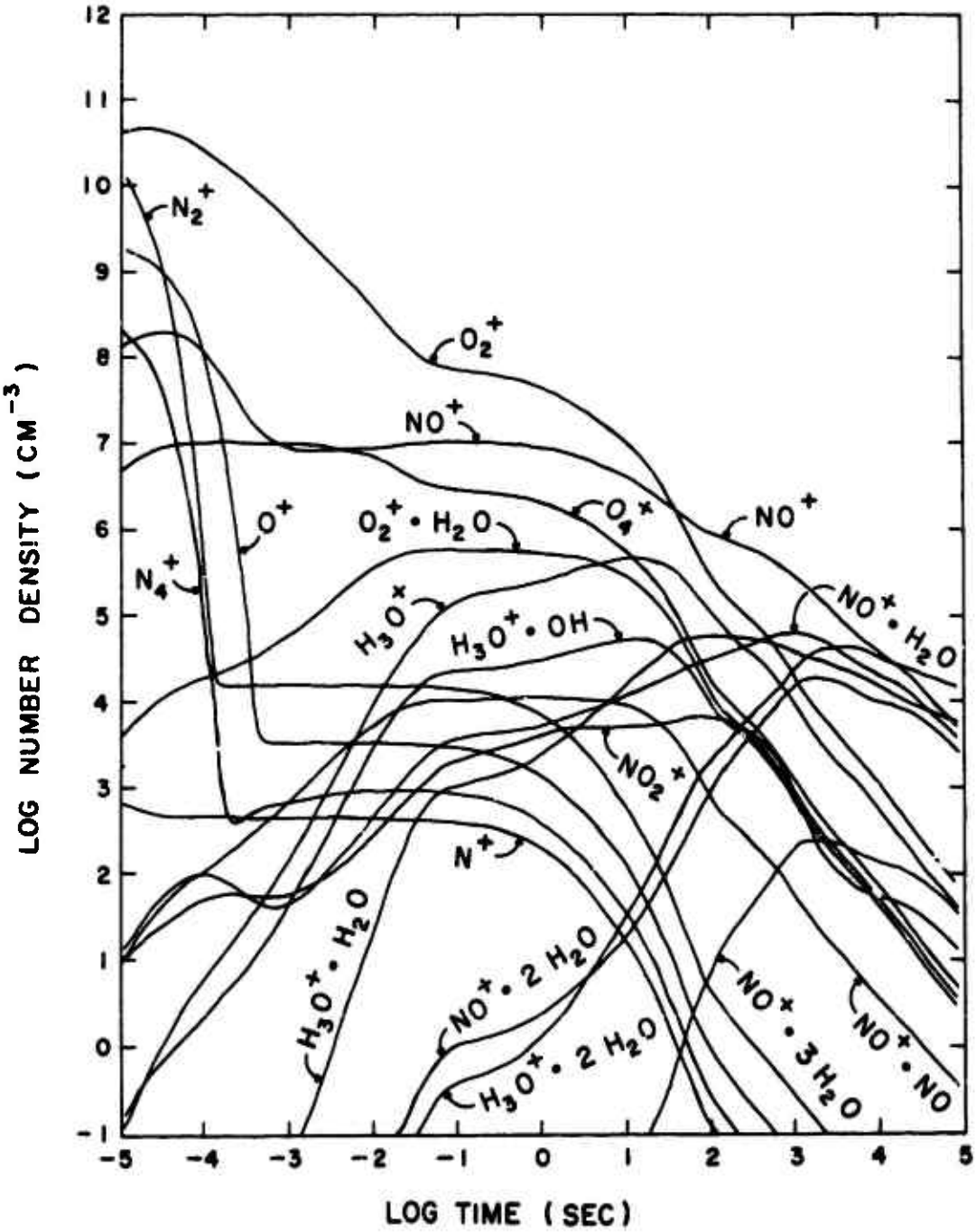

Figure 22-16. Positive-ion densities at 60 km altitude in the beta patch (Reference 22-46).

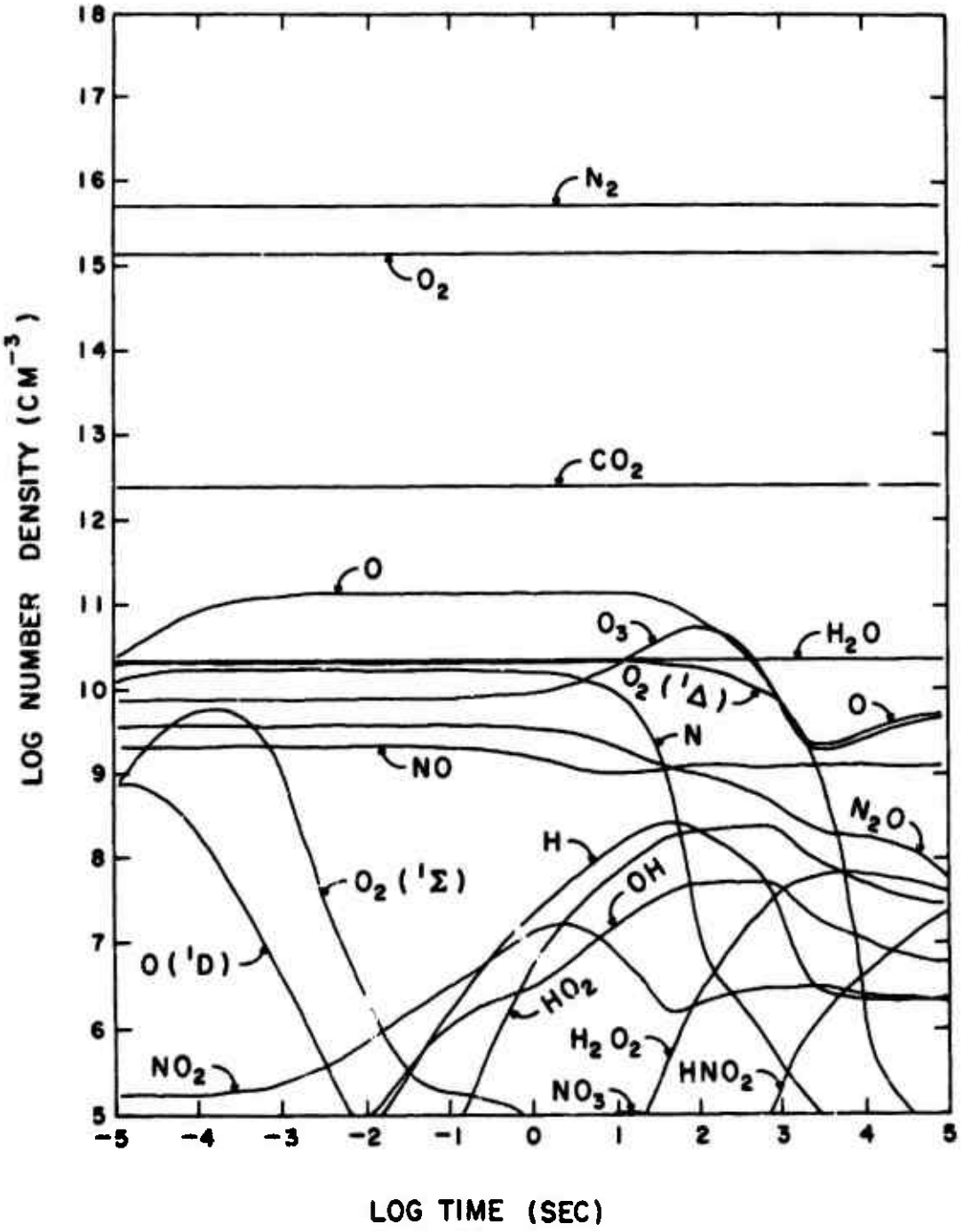

Figure 22-17. Neutral species number densities at 60 km altitude in the beta patch (Reference 22-46).

Figures 22-18 through 22-20 show the comparison of certain species densities, for a high-level ionization, calculated by a detailed multispecies code (solid lines) and analytically (Reference 22-53) (□□, ○○, Δ). Figures 22-21 through 22-23 show the same comparison for a low-level ionization.

The results show that the analytic model is fairly good for a high ionization level but not as good for low ionization levels.

22.4 LUMPED-PARAMETER METHOD

The utilization of multispecies codes can involve prohibitive levels of effort, at least at the present stage of code and machine development, in problems where deionization calculations are required for a very large number of points in space and time. Therefore, approximations are in order for a large group of problems where one can thereby reduce computational time requirements appreciably. Several approaches were discussed earlier, e.g., the elimination of certain species and reactions which have negligible effects on the quantities being computed. For electron density calculations, Lewis and Ali (Reference 22-43) have shown that for the E and F regions, one can obtain accurate results (less than 20 percent error) using a simpler code (See Figures 22-7 and 22-8). For the D region, Scheibe (Reference 22-53) has decoupled the charged chemistry from the neutral-species chemistry and has used steady-state relations to obtain the appropriate concentrations. For electron-density calculations his approximations give rather good results, at least for a high level of ionization (Figure 22-20). Simplified D-region deionization models for nuclear environments based on eliminating specified species and reactions have also been described by Bortner and Galbraith (Reference 22-49), and Ory and Gilmore (Reference 22-54).

Another approach to the reduction of deionization computation times is to lump those species together for which effective rate coefficients can be determined. This method has been used extensively in systems studies. Knapp (Reference 22-55) has recently developed a model for the disturbed D region using the lumped-parameter method.

Deionization models in which species are lumped together and effective reaction rate constants are used have been described extensively in the literature (References 22-56 through 22-62). For

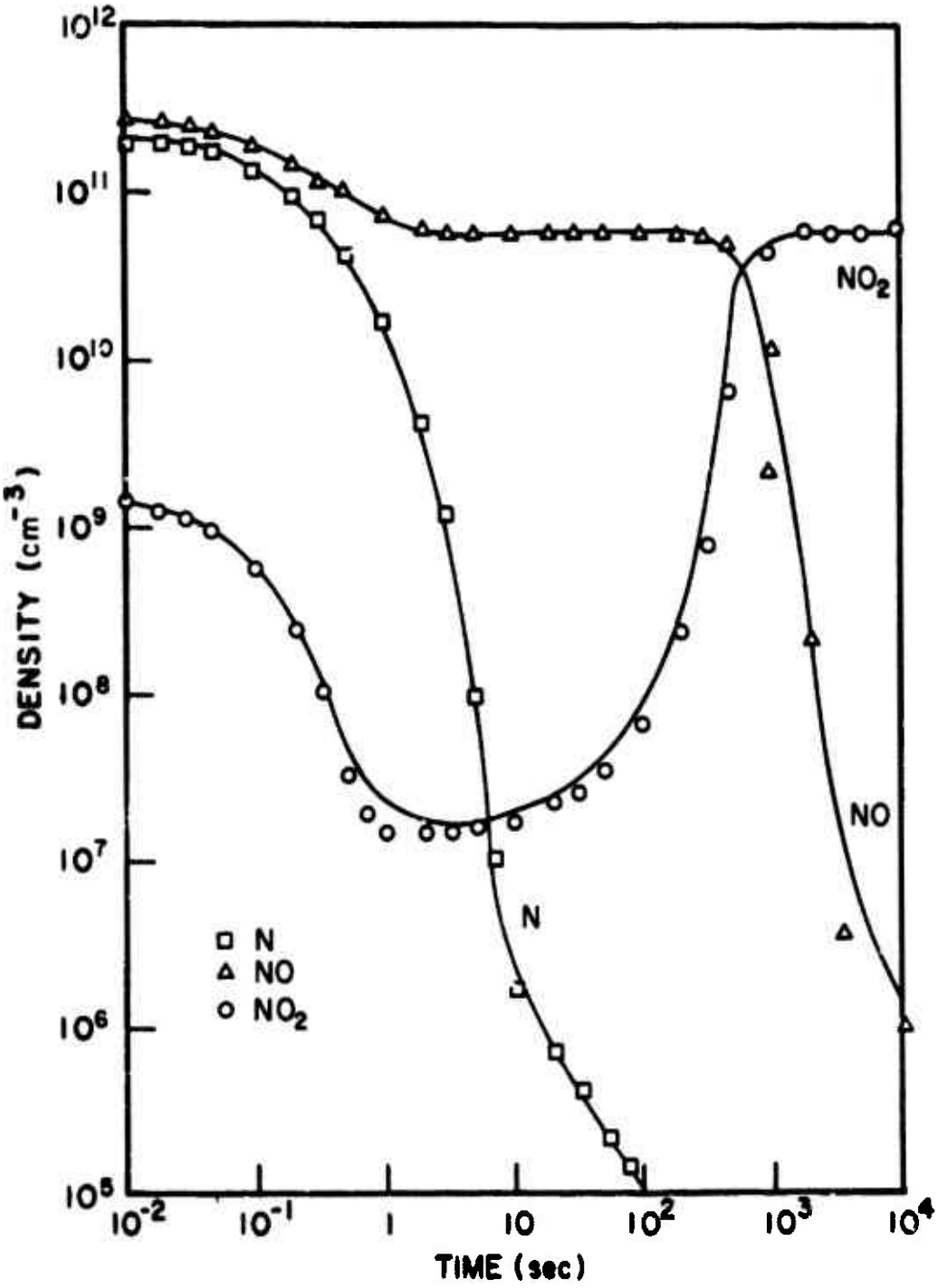

Figure 22-18. Sixty-km, high-level ionization (smooth curve, detailed multi-species code; ○○ △ □, analytic model) (Reference 22-53).

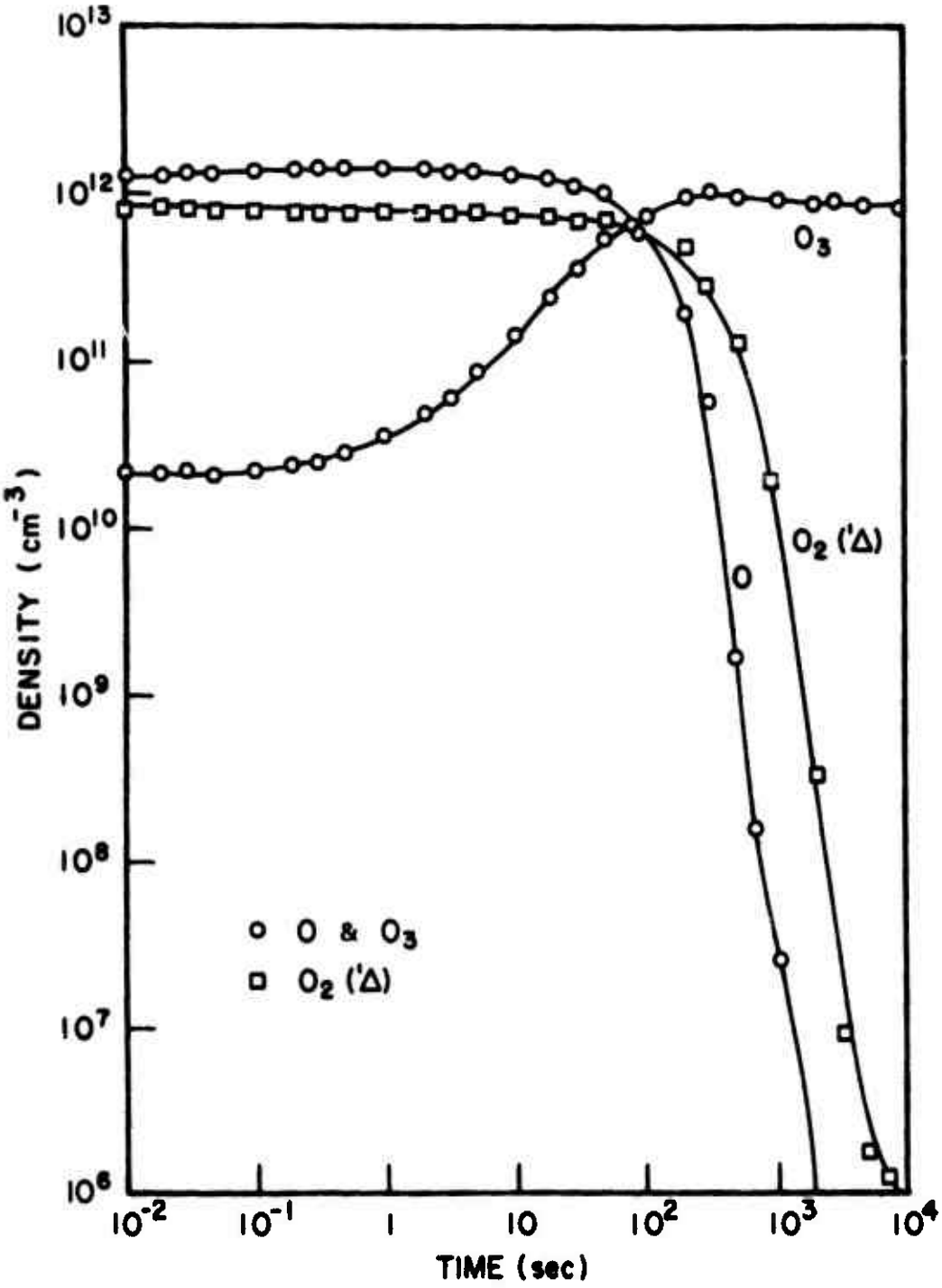

Figure 22-19. Sixty-km, high-level ionizotion (smooth curve, detailed multi-species code; ○ □, onolytic model) (Reference 22-53).

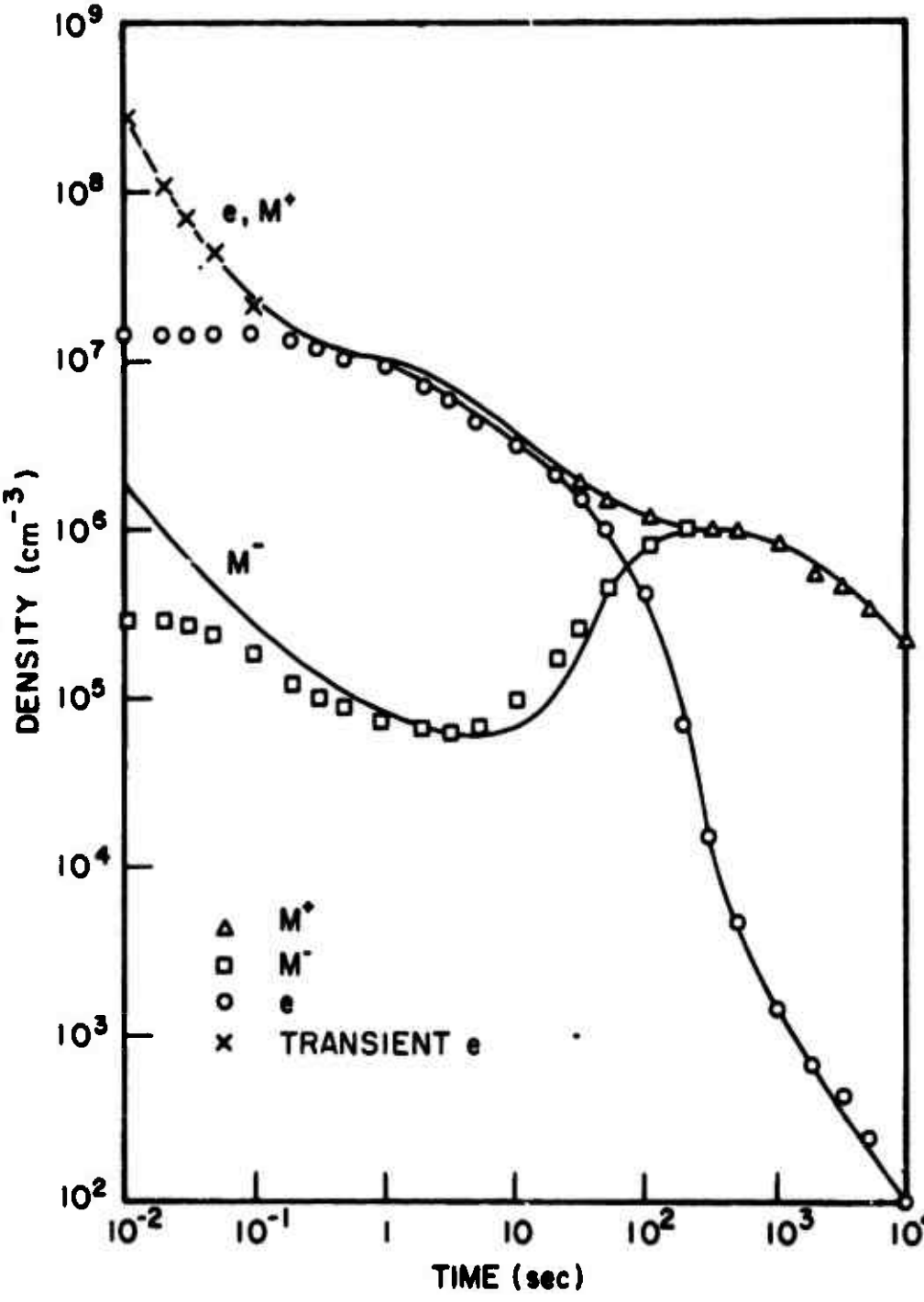

Figure 22-20. Sixty-km, high-level ionization (smooth curve, detailed multi-species code; Δ □ ○ X, analytic model) (Reference 22-53).

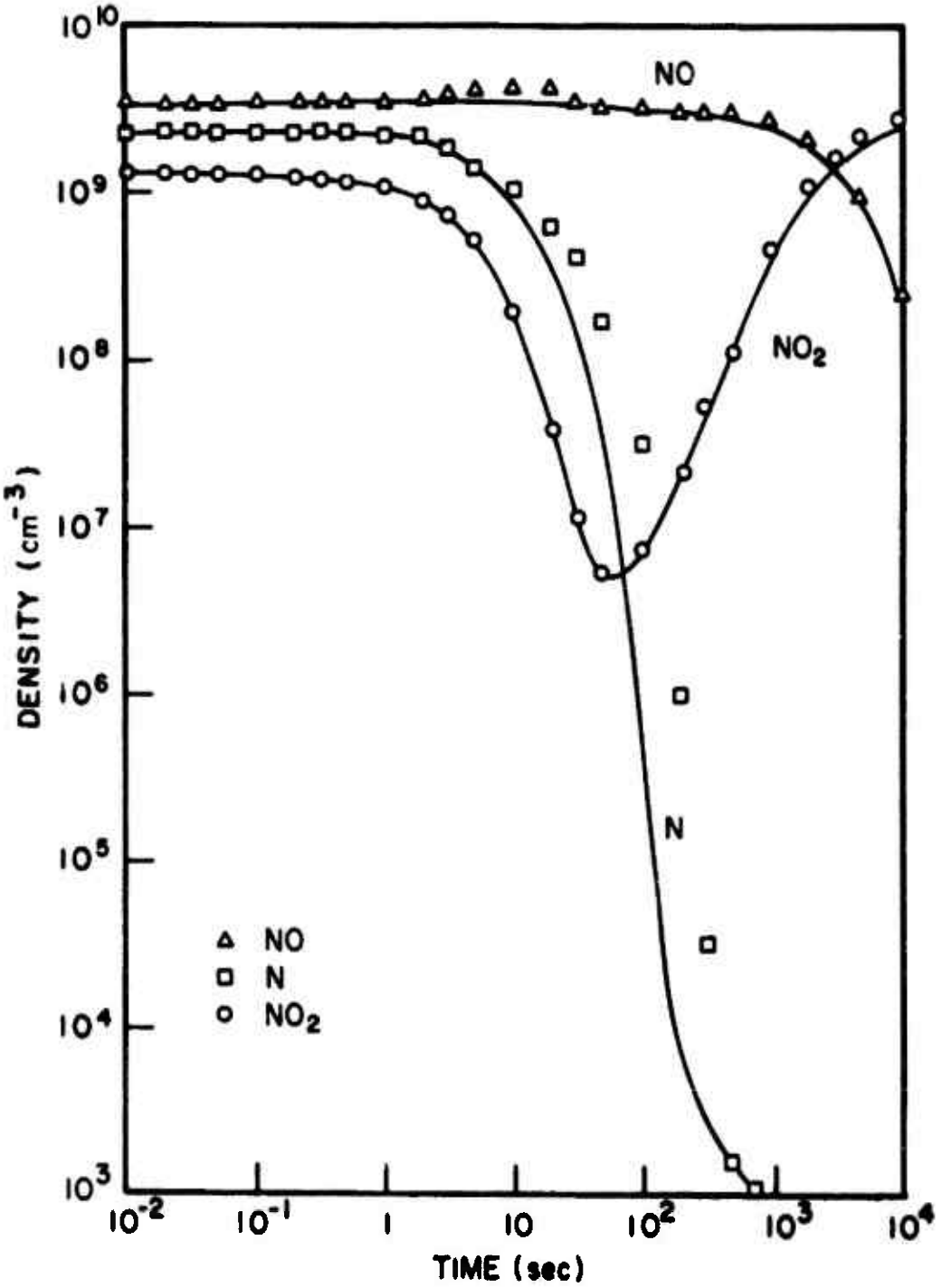

Figure 22-21. Sixty-km, low-level ionizotion (smooth curve, detoiled multi-species code; Δ □ ○, onolytic model) (Reference 22-53).

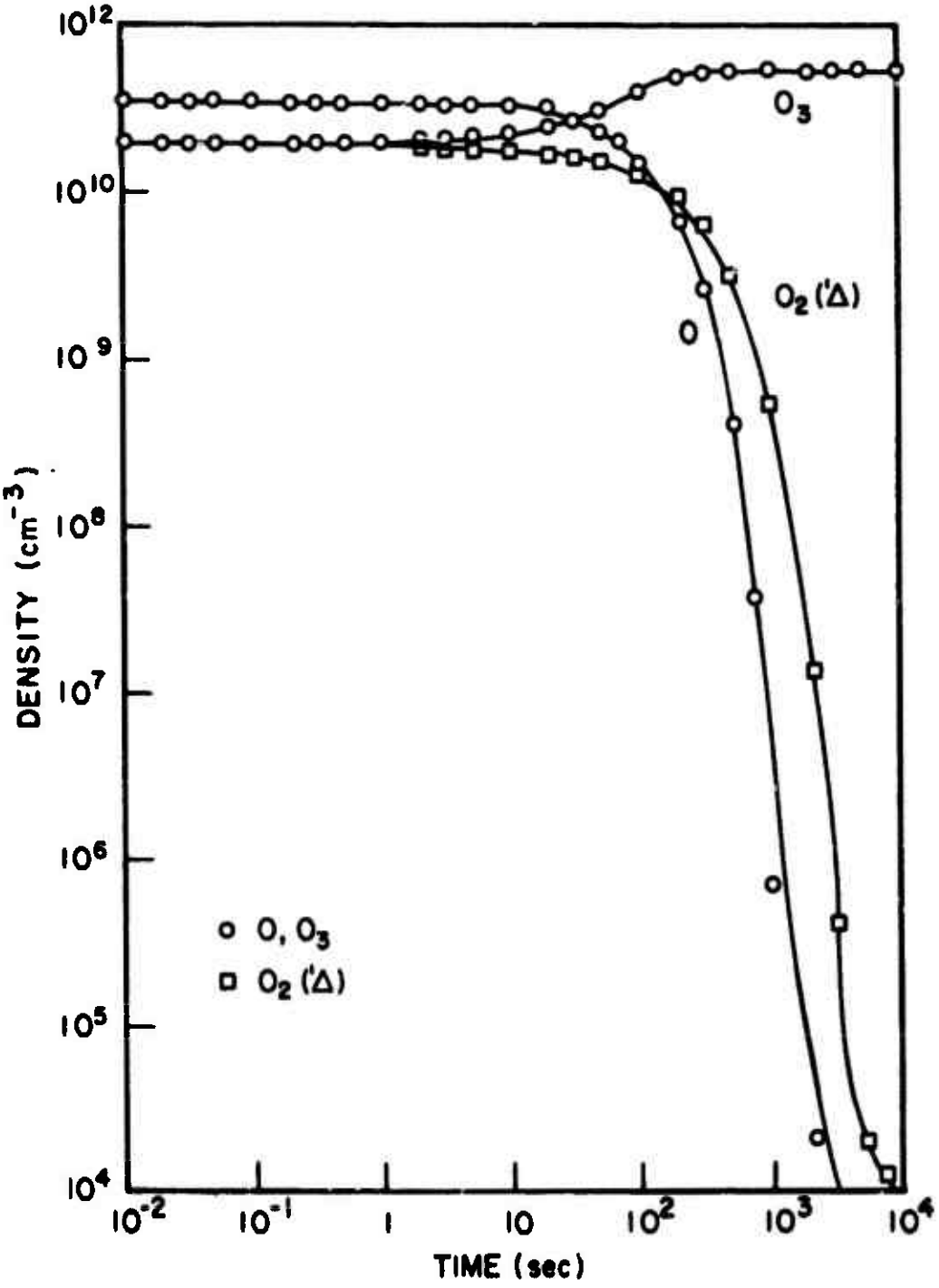

Figure 22-22. Sixty-km, low-level ionization (smooth curve, detailed multi-species code; ○ □, analytic model) (Reference 22-53).

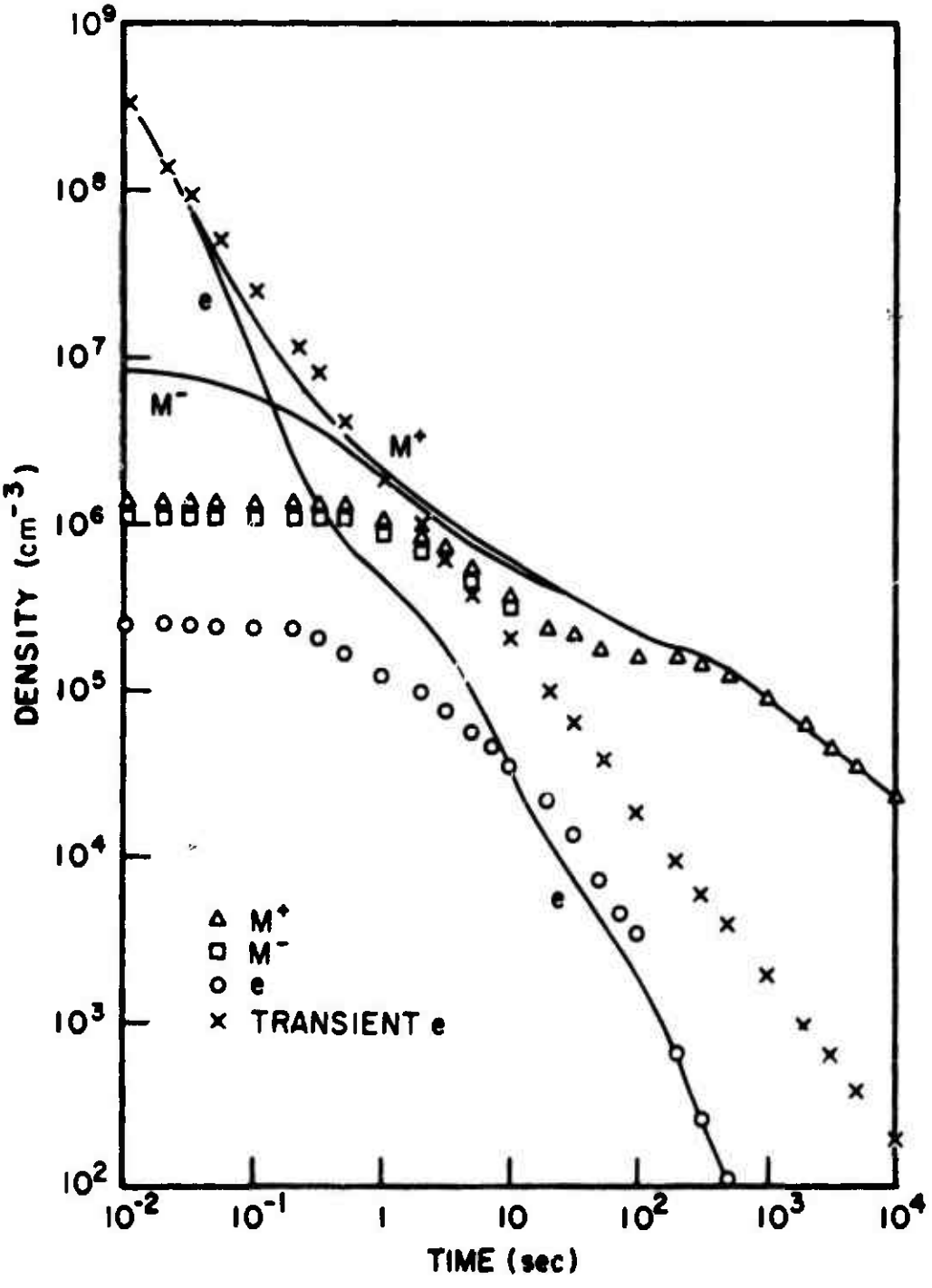

Figure 22-23. Sixty-km, low-level ionization (smooth curve, detailed multi-species code; Δ □ ⌒, analytic model) (Reference 22-53).

altitudes below about 100 km a three-charged-species model has been used for radar and communication system studies. In this model a single representative positive-ion species and a single representative negative-ion species are used and the neutral species are considered to comprise an unchanging background. The reactions considered are electron attachment, electron detachment, electron recombination to positive ions, and ion-ion mutual neutralization. The differential equations describing the species densities are:

$$\frac{dn_e}{dt} = q - \alpha_d n_e n_+ - An_e + Dn_- \qquad (22\text{-}22)$$

$$\frac{dn_-}{dt} = -\alpha_i n_- n_+ + An_e - Dn_- \qquad (22\text{-}23)$$

$$\frac{dn_+}{dt} = q - \alpha_d n_e n_+ - \alpha_i n_- n_+ \qquad (22\text{-}24)$$

where:

n_e = number density of electrons

n_+ = number density of positive ions

n_- = number density of negative ions

A = attachment rate of electrons to neutrals

D = detachment rate of electrons from negative ions

α_d = recombination rate coefficient of electrons and positive ions

α_i = mutual neutralization rate coefficient of positive and negative ions

q = electron-positive ion production rate.

All reaction rates are functions of temperature and neutral species densities at least. The ionization source q is a function of time and space. Equations (22-22) through (22-24) represent only two independent relations since charge neutrality ($n_+ = n_e + n_-$) must be preserved.

Since the lumped rate coefficients comprise a combination of individual rate coefficients for the large number of species actually present, the general problem of finding overall reaction rates as a function of time requires solution of the complete set of differential equations. The lumped-parameter model is most useful when the physical approximation is made that the lumped rate coefficients are independent of time and initial conditions. This approximation can only be justified either by determining from detailed multispecies calculations that for a specified range of conditions the lumped coefficients are essentially constant or by determining a set of coefficients that provide empirical agreement with atmospheric data for a specified range of conditions. The latter approach has been used in determining lumped-parameter reaction-rate models where electron density and total ion density were the principal quantities of interest.

While the lumped-parameter model has significant limitations and must be used with caution, its use can be justified in a number of applications. It has been possible to derive reaction rates which provide reasonable agreement with detailed calculations and ionization conditions of interest in radar and communication system studies. The lumped-parameter model is simple enough to provide a physical understanding of the ionization as a function of altitude and ionization conditions. Mathematical approximations can be made which provide solutions to the lumped-parameter differential equations which are in some cases thousands or even millions of times faster than the complete solution of the multispecies equations.

The principal limitation of the lumped-parameter model is its range of applicability. When the reaction rates are assumed to be only a function of altitude the model will not account for changes in the dominant ion species with ionization conditions. The formation of minor neutral species during the initial energy deposition and subsequent deionization can significantly modify the effective recombination and detachment rates.

The three-ion-species differential equations can be solved in closed form if it is assumed that $\alpha = \alpha_d = \alpha_i$ and q is a constant. For the general case where $\alpha_d \neq \alpha_i$ approximate mathematical solutions of the differential equations have been developed by Bogusch (Reference 22-59) and by Ek (Reference 22-60). For conditions where q varies slowly enough with time so that after the initial

transients die out the ion densities approach a condition where they are essentially in equilibrium with q at any given instant the following quasi-equilibrium solutions can be used:

$$n_+ = \sqrt{\frac{q}{\alpha_e}} \tag{22-25}$$

$$n_e = \frac{q + D\sqrt{\frac{q}{\alpha_e}}}{A + D + \alpha_d\sqrt{\frac{q}{\alpha_e}}} \tag{22-26}$$

$$\alpha_e = \frac{A\alpha_i + D\alpha_d + \alpha_i\alpha_d\sqrt{\frac{q}{\alpha_e}}}{A + D + \alpha_i\sqrt{\frac{q}{\alpha_e}}} \; . \tag{22-27}$$

The relation for determining the effective recombination coefficient α_e (a cubic in α_e) may be solved directly, or an iterative procedure may be used. The quasi-equilibrium solution is often written in terms of λ, the ratio of negative-ion to electron densities instead of α_e (Reference 22-63):

$$n = (1 + \lambda)n_e \tag{22-28}$$

$$n_e = \left[\frac{q}{(1 + \lambda)(\alpha_d + \lambda\alpha_i)}\right]^{1/2} \tag{22-29}$$

$$\lambda = \frac{n_-}{n_e} = \frac{A}{D + \alpha_i(1 + \lambda)n_e} \; . \tag{22-30}$$

Table 22-5 shows reaction rates and coefficients chosen for use with the lumped-parameter model in appropriate studies (Reference 22-61). The values given are consistent with laboratory measurements for diatomic ions. As discussed in Chapters 2 and 5 the dominant atmospheric ions below about 80 km for moderate to low

Table 22-5. Lumped-parameter reaction rate model.

Altitude (km)	Night				Doy			
	A	D	α_d	α_i	A	D	α_d	α_i
0	6.0 (7)		3.0(-7)	4.3(-6)	6.0 (7)	1 (-2)	3.0(-7)	4.3(-6)
5	1.8 (7)		3.0(-7)	3.1(-6)	1.8 (7)	1 (-2)	3.0(-7)	3.1(-6)
10	4.5 (6)		3.0(-7)	2.2(-6)	4.5 (6)	1 (-2)	3.0(-7)	2.2(-6)
15	9.5 (5)		3.0(-7)	1.1(-6)	9.5 (5)	1 (-2)	3.0(-7)	1.1(-6)
20	2.0 (5)		3.0(-7)	5.1(-7)	2.0 (5)	1 (-2)	3.0(-7)	5.1(-7)
25	4.2 (4)		3.0(-7)	2.4(-7)	4.2 (4)	1 (-2)	3.0(-7)	2.4(-7)
30	9.2 (3)		3.0(-7)	1.2(-7)	9.2 (3)	1 (-2)	3.0(-7)	1.2(-7)
35	2.1 (3)		3.0(-7)	7.0(-8)	2.1 (3)	1 (-2)	3.0(-7)	7.0(-8)
40	5.2 (2)		3.0(-7)	4.7(-8)	5.2 (2)	1 (-2)	3.0(-7)	4.7(-8)
45	1.4 (2)		3.0(-7)	3.8(-8)	1.4 (2)	1 (-2)	3.0(-7)	3.8(-8)
50	4.0 (1)		3.0(-7)	3.4(-8)	4.0 (1)	1 (-2)	3.0(-7)	3.4(-8)
55	1.2 (1)		3.0(-7)	3.2(-8)	1.2 (1)	7.0(-2)	3.0(-7)	3.2(-8)
60	3.1 (0)		3.0(-7)	3.1(-8)	3.1 (0)	5.0(-1)	3.0(-7)	3.1(-8)
65	8.0(-1)	1.2(-12)	3.0(-7)	3.1(-8)	7.6(-1)	5.0(-1)	3.0(-7)	3.1(-8)
70	2.2(-1)	1.4 (-5)	3.0(-7)	3.0(-8)	1.7(-1)	5.0(-1)	3.0(-7)	3.0(-8)
75	8.5(-2)	1.2 (-3)	3.0(-7)	3.0(-8)	3.5(-2)	5.0(-1)	3.0(-7)	3.0(-8)
80	3.0(-2)	4.6 (-3)	3.0(-7)	3.0(-8)	6.3(-3)	5.0(-1)	3.0(-7)	3.0(-8)
85	8.5(-3)	9.7 (-3)	3.0(-7)	3.0(-8)	1.2(-3)	5.0(-1)	3.0(-7)	3.0(-8)
90	2.7(-3)	1.9 (-2)	3.0(-7)	3.0(-8)	3.5(-4)	5.0(-1)	3.0(-7)	3.0(-8)
95	1.4(-3)	4.9 (-2)	3.0(-7)	3.0(-8)	4.7(-4)	5.0(-1)	3.0(-7)	3.0(-8)
100	9.1(-4)	7.5 (-2)	3.0(-7)	3.0(-8)	6.6(-4)	5.0(-1)	3.0(-7)	3.0(-8)

N.B.: Numbers given in the form m(n) correspond to $m \times 10^n$.

ionization levels are hydrated ions. Since hydrated ions have much larger rate constants for dissociative recombination, it would be expected that the reaction rates given in Table 22-5 would only be applicable for moderate to high ionization levels. Figure 22-24 shows comparisons of electron densities obtained using the lumped-parameter model with those obtained through a multispecies code A comparison of the one-way vertical absorption resulting from these electron densities for UliF propagation is shown in Table 22-6. As expected, the lumped-parameter model gives good results for the first few hundred seconds and then overestimates electron densities, owing to the formation of hydrated ions. The comparison shown is not intended to imply that similar agreement will occur for other ionization conditions, since a number of compensating factors are involved which depend on the level of ionization and the altitude of interest.

Table 22-6. One-way vertical attenuation in dB for UHF radars.

	1	10	32	100	316	1000 sec
DETAILED CODE	221	50	11	2.4	0.94	0.35
SIMPLE CODE	271	48	11	2.4	1.0	0.47

A lumped-parameter deionization model in which the reaction rates are dependent on ionization conditions has been developed for use in communication system computer codes. The model, obtained by fitting data obtained from multispecies calculations, is primarily applicable for cases where the minor neutral species composition is not significantly modified by deionization processes, i.e., initial ionization less than about 10^8 ion-pairs cm^{-3} and ion-pair production rates less than about 10^8 ion-pairs cm^{-3} sec^{-1}. Lumped-parameter models for quasi-equilibrium conditions which include several positive and negative ions and effective reaction rates which are functions of both the ion-pair production rate and the dominant minor neutral species are being studied.

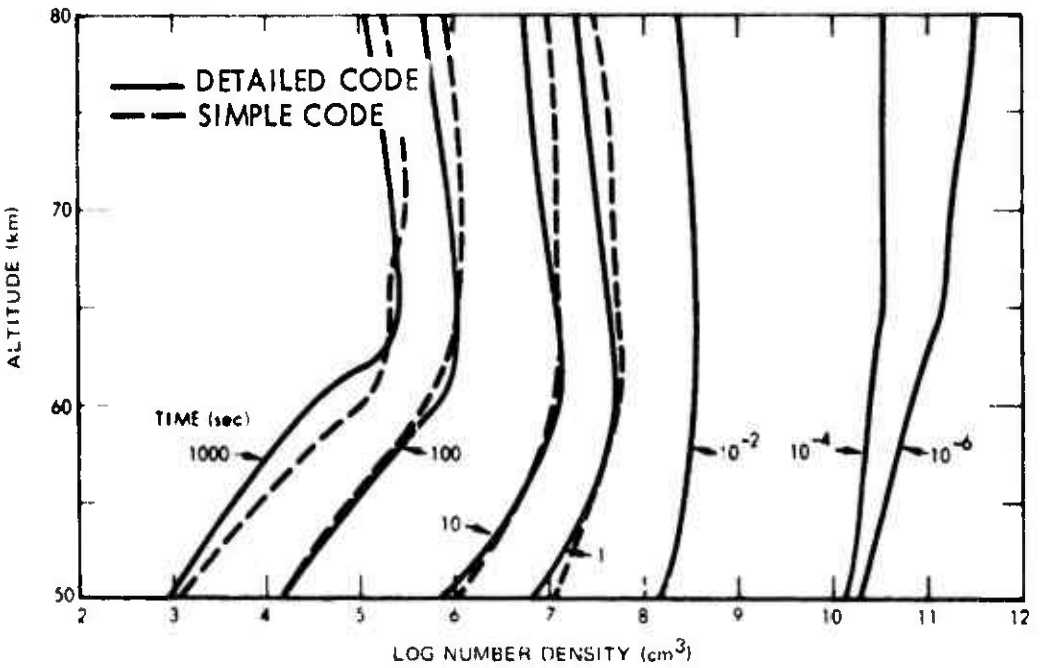

Figure 22-24. Beta-patch electron-density profiles at stated times as calculated by detailed or simple codes (Reference 22-46).

The relationship between the ion-pair production rate and the quasi-equilibrium electron density in the D region is often written in the form:

$$q = \alpha n_e^2 \quad , \tag{22-31}$$

where α is known variously as the steady-state coefficient, effective recombination coefficient, or effective electron loss rate. This form is particularly useful in comparing atmospheric measurements where determinations of q and n_e are made. The quantity α can be expressed in terms of λ or α_e as follows:

$$\alpha = (\alpha_d + \lambda\alpha_i)(1 + \lambda) \quad ; \tag{22-32}$$

$$\alpha = \alpha_e \left(\frac{A + D + \alpha_d \frac{q}{\alpha_e}}{D + \sqrt{q\alpha_e}} \right)^2 \quad . \tag{22-33}$$

Figure 22-25 shows calculations of Ψ obtained from detailed multispecies code data for parametric values of q. At night Ψ has a relatively strong dependence on q. Also shown are atmospheric measurements reported by Megill et al (Reference 22-62) for daytime polar-cap absorption (PCA)* events (q between 10^2 and 10^3 ion-pairs cm^{-3} sec^{-1}). The differences in the theoretical and measured values of Ψ are believed primarily due to missing reactions in the positive-ion cluster chain starting with NO^+, and to differences between the minor neutral species concentrations used in the multispecies code calculations and those actually present at high altitudes.

For altitudes above about 100 km both atomic and molecular positive ions are important and must be modeled separately owing to significantly different loss rates. Simplified models which use a representative molecular positive ion and either a representative atomic positive ion or explicit models of O^+ and N^+ have been developed for use in radar systems computer codes. The reaction rates are formulated in terms of a molecular nitrogen vibrational temperature and an electron temperature which are determined from approximate models for the natural atmosphere and the amount of energy deposited during ionization. The problem of determining deionization in the E and F regions is complicated by atmospheric motion and the effect of deionization on the atomic and molecular

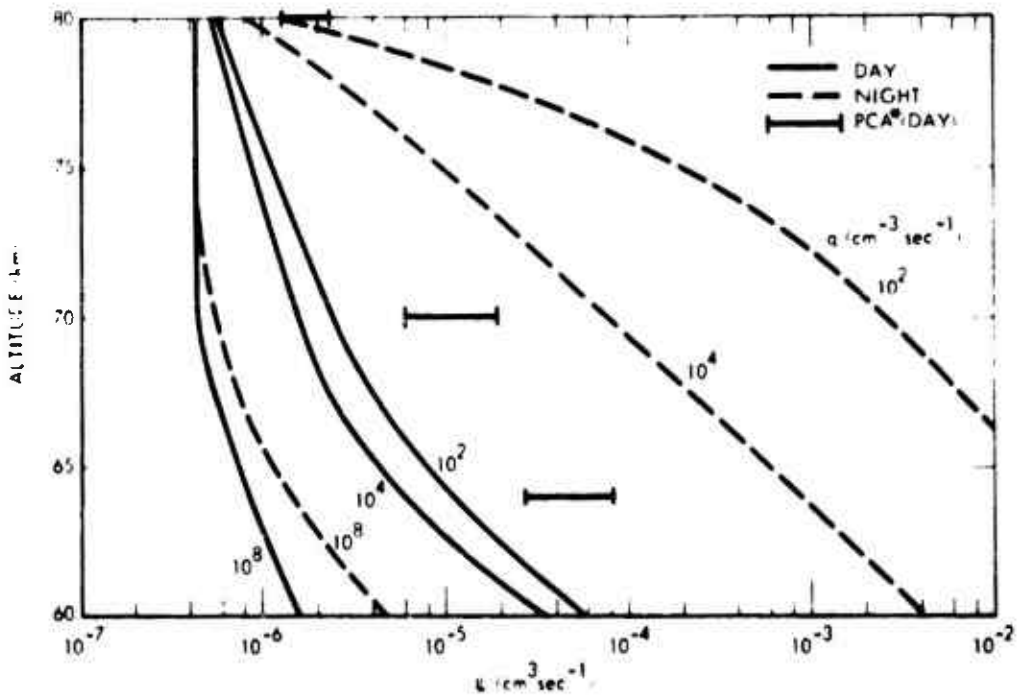

Figure 22-25. Multispecies code colculotions of Ψ.

*Quite recently this phenomenon has come to be known as the Solar Proton Event (SPE).

neutral-species densities. Generally, even when a lumped-parameter model is used, the deionization must be solved sequentially for a series of time steps. Nevertheless, for certain applications the lumped-parameter models are reasonably accurate and are significantly faster than numerical solutions of the differential equations.

REFERENCES

1. Keneshea, T.J., Air Force Cambridge Research Laboratories, Research Report AFCRL-67-0221 (1967).

2. Benyon, P.R., Simulation 11, 219 (1968).

3. Milne, W.E., Numerical Solution of Differential Equations, John Wiley, New York (1953).

4. Kopal, Z., Numerical Analysis, Chapman and Hall, London (1955).

5. Bennett, A.A., W.E. Milne, and H. Bateman, Numerical Integration of Differential Equations, Dover, New York (1956).

6. Hildebrand, F.B., Introduction to Numerical Analysis, McGraw-Hill, New York (1956).

7. Kunz, K.S., Numerical Analysis, McGraw-Hill, New York (1957).

8. Cunningham, W.J., Introduction to Nonlinear Analysis, McGraw-Hill, New York (1958).

9. Ralston, A., and H.S. Wilf, Eds., Mathematical Methods for Digital Computers, John Wiley, New York (1960).

10. Collatz, L., The Numerical Treatment of Differential Equations, Springer-Verlag, Berlin (1960).

11. Lance, G.N., Numerical Methods for High Speed Computers, Illiffe, London (1960).

12. Struble, R.A., Nonlinear Differential Equations, McGraw-Hill, New York (1962).

13. Fox, L., Numerical Solution of Ordinary and Partial Differential Equations...Summer School Held at Oxford, August-September, 1961, Permagon Press, Oxford (1962).

14. Hamming, R.W., Numerical Methods for Scientists and Engineers, McGraw-Hill, New York (1962).

15. Henrici, P., Discrete Variable Methods in Ordinary Differential Equations, John Wiley, New York (1962).

16. Henrici, P., Error Propagation in Difference Methods, John Wiley, New York (1963).

17. Henrici, P., Elements of Numerical Analysis, John Wiley, New York (1964).

18. Davis, P.J., and R. Rabinowitz, Numerical Integration, Blaisdell, Waltham, Mass. (1967).

19. Kelly, L.G., Handbook of Numerical Methods and Applications, Addison-Wesley, Reading, Mass. (1967).

20. Carnahan, B., H.A. Luther, and J.O. Wilkes, Applied Numerical Methods, John Wiley, New York (1969).

21. Lapidus, L., and J.H. Seinfeld, Numerical Solution of Ordinary Differential Equations, Academic Press, New York & London (1971).

22. Treanor, C.E., Computation 20, 39 (1966).

23. Fowler, M.E., and R.M. Warten, IBM Journal 11, 537 (1967).

24. Gear, C.W., Communs. ACM 14, 176, 185 (1971).

25. Kregel, M.D., J. Atm. Terrestr. Phys., to be published (1973).

26. Young, T.R., and J.P. Boris, U.S. Naval Research Laboratory, Memorandum Report 2611 (1973).

27. Mehr, F.J., and M.A. Biondi, Phys. Rev. 181, 264 (1969).

28. O'Malley, T.F., Phys. Rev. 185, 101 (1969).

29. Schmeltekopf, A.L., E.E. Ferguson, and F.C. Fehsenfeld, J. Chem. Phys. 48, 2966 (1968).

30. O'Malley, T.F., J. Chem. Phys. 52, 3269 (1970).

31. Preston, K.F., and R.J. Cvetanovich, J. Chem. Phys. 45, 2888 (1966).

32. Fisher, E.R., and E. Bauer, J. Chem. Phys. 57, 1966 (1972).

33. Hunten, D.M., and M.B. McElroy, Revs. Geophys. 4, 303 (1966).

34. Black, G., and D.J. Eckstrom, Stanford Research Institute, Final Report, Contract DAHC 04-70-C-0036 (1971).

35. Ali, A.W., U.S. Naval Research Laboratory, Plasma Dynamics Tech. Note 32 (1970).

36. Stebbings, R.F., B.R. Turner, and J.A. Rutherford, J. Geophys. Res. 71, 771 (1966).

37. Gilmore, F.R., E. Bauer, and J.W. McGowan, J. Quant. Spectry. Radiative Transfer 9, 157 (1969).

38. Ali, A.W., U.S. Naval Research Laboratory, Plasma Dynamics Tech. Note 20 (1969).

39. Ali, A.W., U.S. Naval Research Laboratory, Plasma Dynamics Tech. Note 24 (1970); DASA Symp. Phys. Chem. Upper Atm., Philadelphia, Pa. (1970).

40. Ali, A.W. et al, U.S. Naval Research Laboratory Report 7578 (1973).

41. Rockwood, S.D. et al, private communication (1971).

42. Lowen, R.W. et al, private communication (1971).

43. Lewis, J., and A.W. Ali, U.S. Naval Research Laboratory, Memorandum Report to be published (1974).

44. Ali, A.W., U.S. Naval Research Laboratory, Plasma Dynamics Tech. Note 42 (1972).

45. Chanin, L.M., A.V. Phelps, and M.A. Biondi, Phys. Rev. Letts. 2, 344 (1959).

46. Niles, F.E., Ballistic Research Laboratories, Report 1518 (1970).

47. Niles, F.E., Ballistic Research Laboratories, Memorandum Report 2080 (1970).

48. Scheibe, M., Lockheed Missiles and Space Company, Report N-15-68-1 (1968).

49. Bortner, M.H., and H.J. Galbraith, General Electric Space Sciences Laboratory, DASA Report 1667 (1965).

50. Bortner, M.H., and R.H. Kummler, General Electric Space Sciences Laboratory, DASA Report 2407 (1970).

51. Kummler, R.H., and M.H. Bortner, General Electric Space Sciences Laboratory Report R67SD20 (1967).

52. Kennshea, T.J. et al, private communication (1971).

53. Scheibe, M., Mission Research Corporation, Report MRC-R-24, DNA Report 2920F (1972).

54. Ory, H.A., and F.R. Gilmore, R&D Associates, DNA Report 2835T (1971).

55. Knapp, W.S., General Electric-TEMPO, private communication (1972).

56. Crain, C., J. Geophys. Res. 66, 1117 (1961).

57. Cole, R.K., Jr., and E.T. Pierce, J. Geophys. Res. 70, 2735 (1965).

58. Reid, G.C., Revs. Geophys. 2, 311 (1964).

59. Bogusch, R.L., General Electric–TEMPO, Report 65TMP-7 (1965).

60. Ek, F.L., MIT-Lincoln Laboratory, Tech. Note 1966-18 (1966).

61. Knapp, W.S. et al, General Electric–TEMPO, Report 66TMP-18, DASA Report 1765 (1966).

62. Megill, L.R. et al, J. Geophys. Res. 76, 4587 (1971).